DOI: 10.1590/2317-4889201720170045

ARTICLE

Records of Mesoproterozoic taphrogenic events in the eastern basement of the Araçuaí Orogen, southeast Brazil

Registros de eventos tafrogênicos mesoproterozoicos no embasamento do Orógeno Araçuaí, sudeste do Brasil

Tobias Maia Rabelo Fonte-Boa[1]*, Tiago Amâncio Novo[1], Antônio Carlos Pedrosa-Soares[1,3], Ivo Dussin[2,3]

ABSTRACT: The history of palaeocontinents alternates long fragmentation to drift periods with relatively short agglutination intervals. One of the products of a Rhyacian-Orosirian orogeny was a palaeocontinent that brought together the basement of the Araçuaí-West Congo orogen (AWCO) with regions now located in the São Francisco and Congo cratons. From ca. 2 Ga to ca. 0.7 Ga, this large region of the São Francisco-Congo palaeocontinent was spared of orogenic events, but underwent at least five taphrogenic events recorded by anorogenic magmatism and/or sedimentation. The taphrogenic events are well documented in the AWCO proximal portions and neighboring cratonic regions, but lack evidence in the AWCO high-grade core. Our studies on amphibolites intercalated in the Rhyacian Pocrane complex, basement of the Rio Doce magmatic arc, allowed to the recognition of two Mesoproterozoic taphrogenic episodes. The oldest one, a Calymmian episode, is recorded by amphibolites with a zircon magmatic crystallization age at 1529 ± 37 Ma (U-Pb SHRIMP), and lithochemical signature of basaltic magmatism related to continental intraplate settings. Another set of amphibolite bodies records the youngest taphrogenic episode, a Stenian event, with a zircon magmatic crystallization age at 1096 ± 20 Ma (U-Pb SHRIMP), and lithochemical signature similar to mature magmatism of continental rift setting. The Calymmian episode (ca. 1.5 Ga) correlates to the Espinhaço II basin stage and mafic dikes of the northern Espinhaço, Chapada Diamantina and Curaçá domains, while the Stenian episode (ca. 1.1 Ga) correlates to the Espinhaço III basin stage. We also present U-Pb data for 87 detrital zircon grains from a quartzite lens intercalated in the Pocrane complex, the Córrego Ubá quartzite. Its age spectrum shows main peaks at 1176 ± 21 Ma (35%), 1371 ± 30 Ma (18%), 1536 ± 22 Ma (19%), 1803 ± 36 Ma (17%) and 1977 ± 38 Ma (12%), suggesting a Stenian (ca. 1176 Ma) maximum depositional age (although only one zircon with low discordance shows an age of 955 ± 66 Ma). Comparing with data from the western sector of the Araçuaí orogen and São Francisco craton, it is noteworthy that no igneous zircon from the three samples yielded an age older than early Orosirian (~2.05 Ga), showing age spectra essentially limited in the range of ca. 1–2 Ga; i.e., younger

RESUMO: *A história dos paleocontinentes resume-se em longos períodos de fragmentação e pequenos intervalos de aglutinação. Um dos produtos de uma orogenia riaciana-orosiriana foi o paleocontinente São Francisco-Congo, representado nos crátons homônimos e no embasamento do Orógeno Araçuaí-Congo Ocidental (AWCO). Durante o período de ca. 2 Ga até ca. 0,7 Ga, aquela extensa região paleocontinental foi poupada de eventos orogênicos, mas por outro lado foi submetida a pelo menos cinco eventos tafrogênicos registrados por magmatismo anorogênico e sedimentação. Tais eventos tafrogênicos estão bem registrados nas zonas proximais do AWCO e regiões cratônicas adjacentes, mas suas evidências no núcleo de alto grau do AWCO são muito mais raras. Nossos estudos sobre lentes anfibolíticas intercaladas em ortognaisses do Complexo Pocrane, embasamento do Arco Magmático Rio Doce, permitiram reconhecer dois eventos tafrogênicos mesoproterozoicos distintos. O mais antigo deles, do Caliminiano, é caracterizado por anfibolitos com zircões cristalizados em 1529 ± 37 Ma (U-Pb SHRIMP). Outro conjunto de anfibolitos registra episódio tafrogênico mais jovem, do Esteniano, com zircões de idade magmática em 1096 ± 20 Ma (U-Pb SHRIMP). O episódio calimiano (ca. 1,5 Ga) é correlato com a bacia Espinhaço II e diques máficos dos domínios Espinhaço, Chapada Diamantina e Curaçá, enquanto o episódio esteniano (ca. 1,1 Ga) se correlaciona com a bacia Espinhaço III. Dados U-Pb de 87 grãos detríticos de zircão coletados em lentes do Quartzito Córrego Ubá, intercaladas no Complexo Pocrane, mostram um espectro de idades com picos em 1176 ± 21 Ma (35%), 1371 ± 30 Ma (18%), 1536 ± 22 Ma (19%), 1803 ± 36 Ma (17%) e 1977 ± 38 Ma (12%). Apesar de se ter encontrado um zircão com idade de 955 ± 66 Ma, o tratamento estatístico dos dados sugere a idade máxima de deposição em ca. 1176 Ma. O espectro de idades mostra-se essencialmente limitado no intervalo 1–2 Ga, contrastando com os dados do setor oeste do AWCO e do*

[1]Universidade Federal de Minas Gerais, Programa de Pós-graduação em Geologia, CPMTC-IGC, Belo Horizonte (MG), Brazil. *E-mails: tobiasfonteboa@gmail.com, tiagoanovo@gmail.com, pedrosa@pq.cnpq.br*

[2]Universidade Estadual do Rio de Janeiro, Faculdade de Geologia, Rio de Janeiro (RJ), Brazil. *E-mail: ivodusin@yahoo.com.br*

[3]Fellow of the Brazilian Research Council (CNPq).

*Corresponding author.

Manuscript ID: 20170045. **Received on:** 03/29/2017. **Accepted on:** 06/27/2017.

than the Late Rhyacian orogeny that amalgamated the basement, and older than the main anorogenic event (930–870 Ma) associated with the Early Tonian precursor basin of AWCO. All together, these continental taphrogenic events testify the several unsuccessful fragmentation attempts that affected the long-lived São Francisco-Congo palaeocontinent, which remained preserved from a complete break-up associated with ocean spreading from the Early Orosirian to the Atlantic opening in Cretaceous time.

KEYWORDS: Taphrogenic events; São Francisco-Congo palaeocontinent; Araçuaí-West Congo orogeny.

Cráton São Francisco, onde são comuns zircões do Toniano ou mais velhos que 2 Ga. Isso sugere uma bacia alimentada por fontes relativamente restritas. Os dois eventos tafrogênicos mesoproterozoicos aqui reportados evidenciam duas das tentativas de fragmentação mal sucedidas que incidiram sob o Paleocontinente São Francisco-Congo, o qual resistiu à completa fragmentação desde ca. 2 Ga até a abertura do Oceano Atlântico no Cretáceo.

PALAVRAS-CHAVE: *Eventos tafrogênicos; Paleocontinente São Francisco-Congo; Orógeno Araçuaí-Congo Ocidental.*

INTRODUCTION

The history of palaeocontinents includes short compressive orogenic processes, intercalated with large taphrogenic phases marked by fragmentation and drift (Nance *et al.* 1988, Murphy & Nance 1992, Rogers & Santosh 2004). In this context, a new-formed continent becomes a refractory cap that hinders heat release from the Earth's mantle. The heat transmission is associated to magmas, that tend to settle beneath rift systems. The reconstruction of the rifting events is easily detected and characterized when it comes from undeformed domains. However, reconstruction becomes much more complex in orogenetic reworked cores, in which rocks associated with taphrogenic events are intensely deformed. A fundamental tool for the analysis of tectonized magmatism and/or sedimentation is U-Pb dating on zircon grains. Besides the magmatic and metamorphic age, the analyses of the zircon age spectra of sedimentary deposits may reflect the tectonic setting of the basin, providing important hints for tectonic and palaeogeographic interpretations (Cawood *et al.* 2012).

The study area, located in the Araçuaí Orogen, southeastern Brazil (Fig. 1), records a series of events related to the amalgamation of the São Francisco-Congo palaeocontinent in the Rhyacian-Orosirian boundary (Noce *et al.* 2007), as well as the evolution of the Araçuaí Orogen in Neoproterozoic time (Pedrosa-Soares *et al.* 2001, 2008; Alkmim *et al.* 2006). It lacks evidence that the region had experienced orogenic events from the Orosirian to the Ediacaran. Conversely, during that long period, the region between the São Francisco and Congo cratons records at least five major taphrogenic events which ultimately led to the development of the precursor basin system of the Araçuaí Orogen (Pedrosa-Soares & Alkmim 2011, Chemale Jr. *et al.* 2012, Guadagnin *et al.* 2015, Tupinambá *et al.* 2007). Although these anorogenic events are well documented in the proximal zone of the Araçuaí Orogen and in the São Francisco Craton, no solid evidence from them were previously found in the high-grade core of the Araçuaí Orogen.

This paper focuses on metamafic rocks (amphibolites) and the Córrego Ubá quartzite, spatially associated with the Rhyacian Pocrane complex, located in the high-grade core of the Araçuaí Orogen (Fig. 1). Our field, petrographic, lithochemical and geochronological (zircon U-Pb SHRIMP and LA-ICP-MS) studies provide evidence of two distinct Mesoproterozoic taphrogenic events on the Rhyacian basement of the Araçuaí Orogen high-grade core. Based on a thorough compilation of the literature, we correlate these data with the main unsuccessful taphrogenic events which affected the São Francisco-Congo palaeocontinent before the evolution of the Araçuaí Orogen.

GEOLOGICAL SETTING

The Neoproterozoic Araçuaí Orogen together with its counterpart located in Africa, the West Congo Belt, evolved during the Brasiliano cycle, one of the tectonic cycles that led to West Gondwana amalgamation.

The focused area covers part of the basement of the high-grade core of the Araçuaí Orogen (Fig. 1), where the Ediacaran Rio Doce magmatic arc is an outstanding feature and metamorphic peaks ranges from the amphibolite to granulite facies (Novo *et al.* 2010; Tedeschi *et al.* 2015; Gonçalves *et al.* 2015).

The basement includes gneissic-migmatitic complexes in the amphibolite (e.g., the Pocrane Complex; Novo 2013) to granulite facies (e.g., the Juiz de Fora Complex; Noce *et al.* 2007). Those complexes formed in response to convergence related to an orogenic Rhyacian-Orosirian event that amalgamated the São Francisco-Congo palaeocontinent (Noce *et al.* 2007; Heilbron *et al.* 2010; Silva *et al.* 2016). After the basement consolidation, the region seems to have experienced a long period without any event of compressive nature (Pedrosa-Soares *et al.* 2001, 2008, 2011; Pedrosa-Soares & Alkmim 2011), until the onset of the Brasiliano orogeny in Early Ediacaran (Novo *et al.* 2010; Pedrosa-Soares *et al.* 2011; Tedeschi *et al.* 2015).

Pocrane Complex

The Pocrane Complex is mainly composed of tonalite-trondhjemite-granodiorite (TTG) orthogneiss

with migmatitic portions. Stricto sensu amphibolite lenses (Fig. 2) usually occur interlayered in this gneiss (Silva *et al.* 1987; Novo 2013), as sills or tectonic slices. Previous reports on these metamafic rocks (Paes 1999, Silva *et al.* 2002) point out the variability of their genesis. In the available geological maps (Tuller 2000; Féboli & Paes 2000; Oliveira 2000), lenses and layers of ultramafic and metasedimentary rocks (e.g., calcissilicatic rock, mica schist, paragneiss, quartzites, marble and paraconglomerate) were described as intercalations in the Pocrane Complex orthogneiss. The structural pattern of the metasedimentary layers delineates a large fold with a plunging axis in the NNE-SSW direction and hinge concavity facing SSW. At first, the available geological data suggests that the lithological set (orthogneiss, metamafic and metasedimentary layers) should be a bundle of interpolations of igneous and sedimentary origins, simultaneously folded as a deformed and metamorphosed volcano-sedimentary sequence. However, the new data presented in this paper refuses this theory (of one single volcano-sedimentary association), showing that at least part of the metamafic rocks and the sedimentary strata is younger than the orthogneiss.

Córrego Ubá quartzite

The Córrego Ubá quartzite occurs as a tectonic slice interlayered in the Pocrane Complex gneiss (Ubá Creek Cross Section in Fig. 2). It is a fine-grained and recrystallized quartzite that shows three foliation sets, whose main one (S_n) is marked by biotite and muscovite, north-south trend and moderate deep to east. Near tectonic contacts, the foliation develops a mylonitic texture. The biotite enrichment confers a strongly folded and crenulated gneiss banding marking S_{n+1}. A brittle deformation crosscuts all the previous structures materializing S_{n+2}. The quartzite is mainly composed by quartz with granoblastic polygonal texture and accessory biotite, muscovite, plagioclase, titanite and zircon.

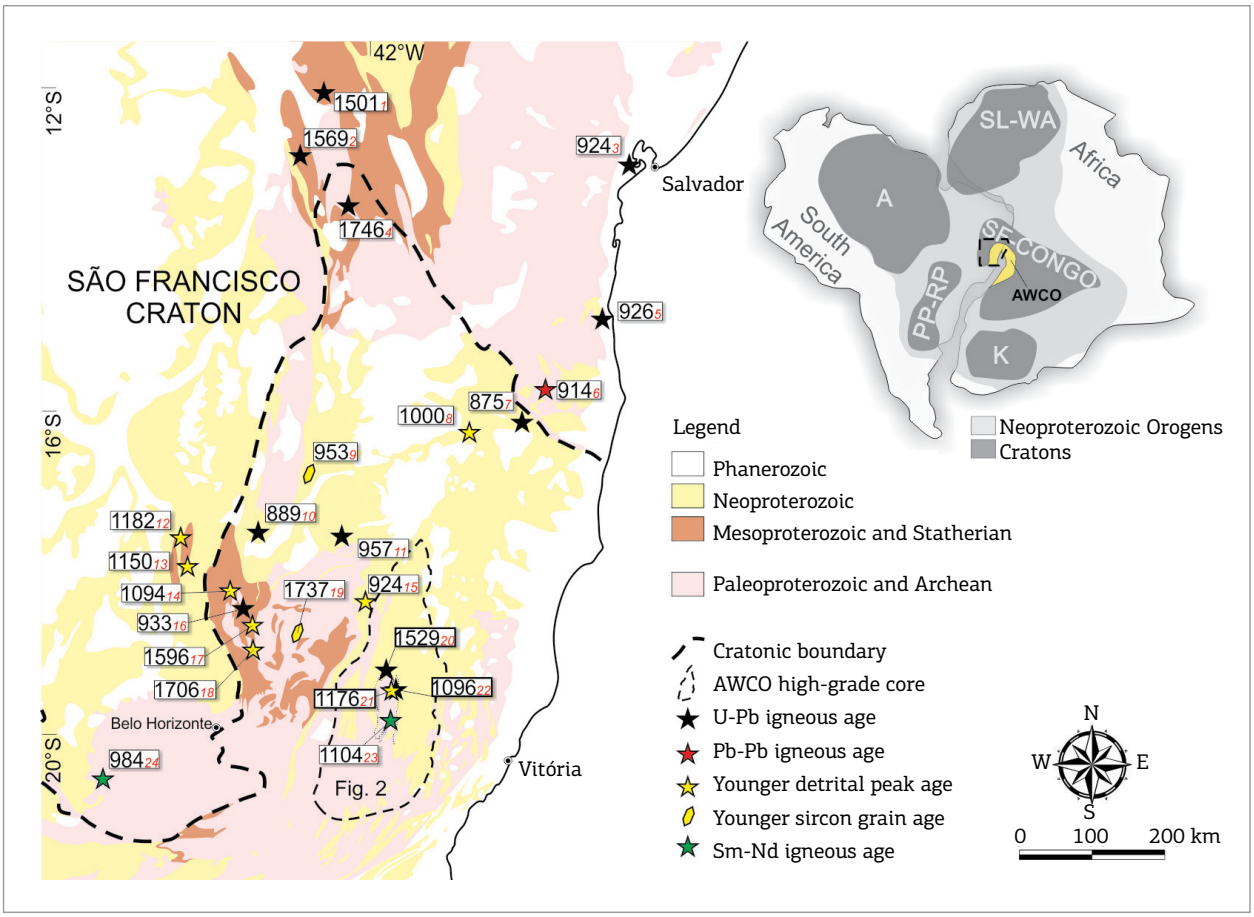

Figure 1. Tectonic situation of the São Francisco Craton and the neighbor orogens. Ages shown in the map are from: 1) Silveira *et al.* 2013; 2) Danderfer *et al.* 2009; 3) Evans *et al.* 2015; 4) Lobato *et al.* 2015; 5) Evans *et al.* 2015; 6) Menezes *et al.* 2012; 7) Silva *et al.* 2002; 8) Gonçalves-Dias *et al.* 2016; 9) Kuchenbecker *et al.* 2015b; 10) Souza 2016; 11) Castro *et al.* 2015; 12) Dussin 2016; 13) Kuchenbecker *et al.* 2015a; 14) Chemale Jr. *et al.* 2012; 15) Peixoto *et al.* 2015; 16) Dussin & Chemale Jr. 2012; 17) Silveira 2016; 18) Rolim *et al.* 2016; 19) Barrote 2016; 20) This Work; 21) This Work; 22) This Work; 23) Angeli *et al.* 2004; 24) Chaves 2001.

Amphibolite lenses

The amphibolites we focus on outcrop as thick lenses (Fig. 2) with low lateral continuity (not more than six meters) interlayered with the Pocrane Complex gneiss. They show fine-grained and compact aspect, though foliation is visible with a magnifying glass and in thin section, or in partially weathered outcrops. The amphibolite consists of hornblende, plagioclase, biotite, quartz, chlorite, apatite, titanite, zircon and opaque minerals (Fig. 3). Biotite and chlorite are formed by hornblende alterations; biotite may be more abundant than hornblende. The foliation (Sn) of amphibolites is anastomosed, developed from a progressive deformational phase. Sometimes late ductile shear zones obliterate the foliation. Amphibole crystals and

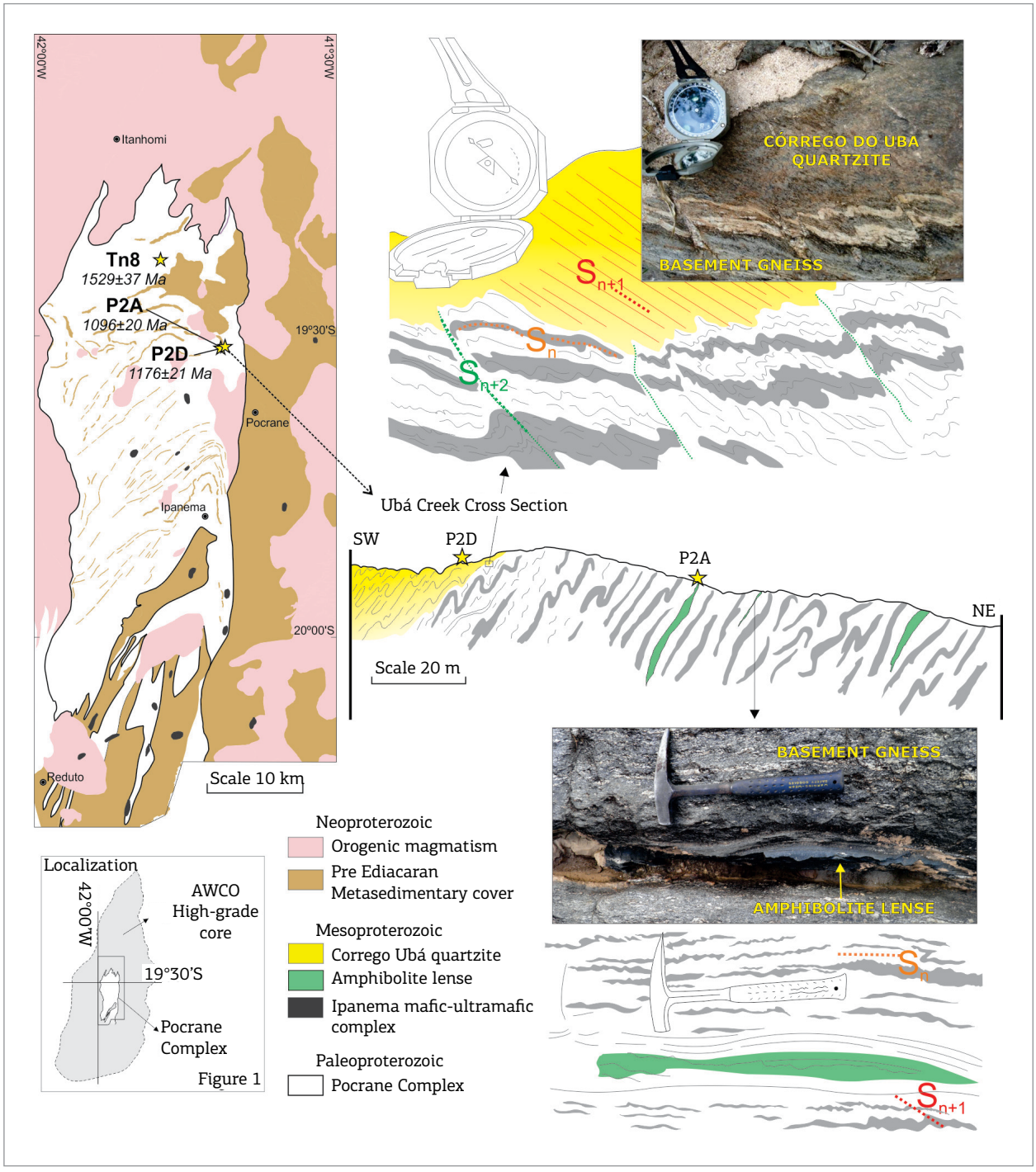

Figure 2. Geological map of the Pocrane Complex and the Córrego Ubá Cross Section showing the field aspects of the Córrego Ubá quartzite and amphibolite lenses. Yellow star marks the sample site location.

biotite palettes materialize the foliation, and the stretched amphibole crystals commonly form ocellar porphyroclasts, showing pressure shadows and recrystallization tails. Quartz and plagioclase occur as stretched crystals, parallel to the foliation, and may display dynamic recrystallization with subgrains individualization.

AMPHIBOLITE LITHOCHEMISTRY

Analytical procedures

The whole-rock lithochemical analyses were conducted on three samples from distinct amphibolite lenses: TN-8A, TN-8B and P2A (Fig. 2). Sample powders were analyzed by Geosol Laboratories, in Belo Horizonte, Brazil. Major and trace element contents were determined using inductively coupled plasma optical emission spectroscopy (ICP-OS/MS) and inductively coupled plasma mass spectrometry (ICP-MS), respectively. Detection limits are 0.01% for oxides and 0.1 ppm for most trace elements, reaching values up to 0.01 ppm for Heavy Rare Earth Elements (HREE), such as Tb, Tm and Lu. The lithochemical analyses are available in the Supplementary data file labeled as "Lithochemical_Data".

Results

Whole-rock chemical analyses were performed for major and trace elements of three samples of amphibolite lenses. Although the data are not sufficient for a statistical analysis, the analytical results provide a preliminary approach.

Classification diagrams for the magmatic protoliths of amphibolites indicate tholeiitic gabbro and sub-alkaline compositions (Figs. 4A and 4B). The Rare Earth Elements (REE) patterns distribution shows that samples TN-8A and TN-8B are markedly different from sample P2A (Fig. 4C). Sample P2A is low fractionated and very little depleted in Light Rare Earth Elements (LREE) [(La/Yb)n = 0.63], meanwhile Samples TN-8A and TN-8B are, on the whole, enriched in REE [(La/Yb)n = 2.91 – 7.39]; they show remarkable fractionation, with enrichment of LREE in relation to HREE.

The lithochemistry presented here reflects the different amphibolites under study. Despite their field and petrographic similarities, their ages are different, as shown ahead.

GEOCHRONOLOGY

Two samples of amphibolites lenses were prepared and analyzed for U-Pb isotopes in the *Centro de Pesquisas Geocronológicas* (CPGeo), São Paulo University, Brazil, by using the sensitive high-resolution ion microprobe (SHRIMP IIe) equipment. One sample from Córrego Ubá quartzite was prepared and analyzed for U-Pb isotopes by using the laser ablasion multicollector inductively coupled plasma mass spectrometry (LAMC-ICP-MS) equipment in the CPGeo, São Paulo University, Brazil.

Material and Methods

About 20 to 40 kg of each rock sample, as for quartzite and amphibolite, were prepared for analyses in laboratories

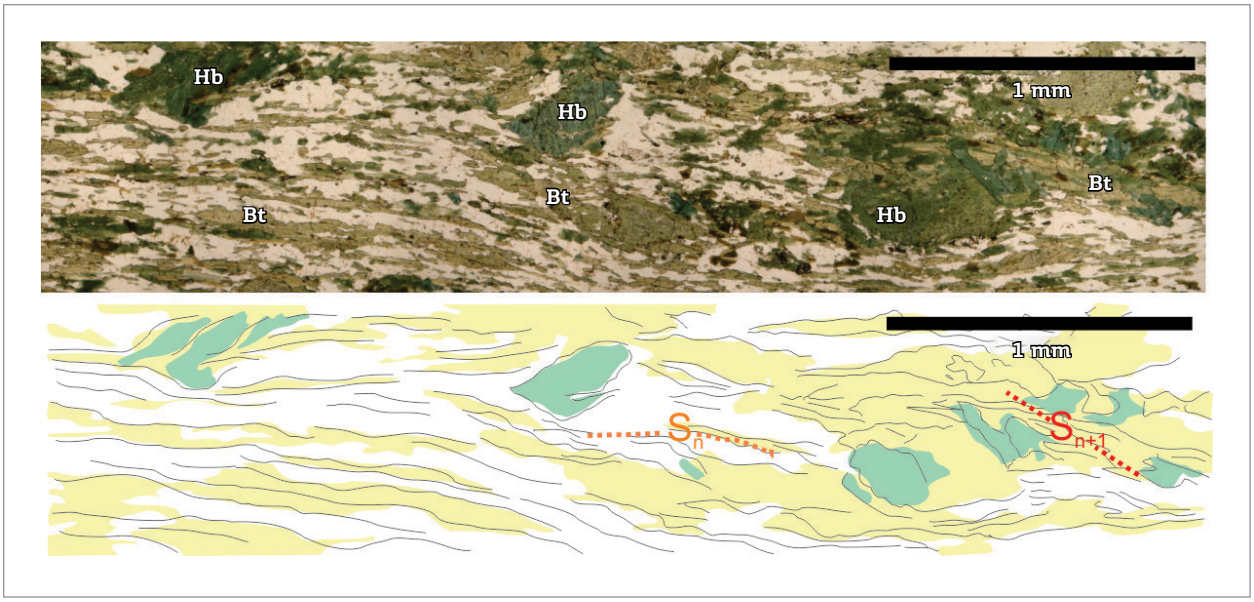

Figure 3. Amphibolite microscopic aspects: Sn and Sn+1 foliation outlined by hornblende and biotite, which envelops hornblende porphyroclast.

of São Paulo University, Brazil. Zircon grains were separated using conventional methods (crushing, grinding, gravimetric and magnetic-Frantz isodynamic separator) and hand-picked under binocular microscope. For geochronological analysis of the magmatic rocks and their metamorphic equivalents, zircon crystals from the least magnetic fractions were selected. After mounted in epoxy disks and polished to expose grain centers, backscattered electron (BSE) and cathodoluminescence (CL) images revealed morphological features and internal structures of zircon grains. No analytical spot was performed on grain areas with inclusions, fractures and/or metamict features. Temora (417 Ma; Black *et al.* 2003) standard zircon was used in SHRIMP and M127 (Klötzli *et al.* 2009) and Plešovice (Sláma *et al.* 2008) standard zircons were used in LAMC-ICP-MS analytical routines. In this study, the spot size in SHRIMP analyses had 30 and 25 μm — LAMC-ICP-MS. Data reduction used the SQUID software (Ludwig 2003) for the SHRIMP data, and Glitter software (Van Achterbergh *et al.* 2001) and the Excel sheet developed by Ludwig (2003) for the LAMC-ICPMS data. Data evaluation for each spot took into account the common Pb contents, errors of isotopic ratios, percentages of discordance and Th/U ratios. From the selected spots, only those with discordance of lesser than 10% were used to age calculations and plotted in histograms and Concordia diagrams. The Concordia diagram and histograms were obtained with the Isoplot/Ex software (Ludwig 2003).

Only zircon crystals from the least magnetic fractions were selected from samples P2A and TN-8A (amphibolite lenses that occur interlayered in the Pocrane Complex orthogneiss). For the Córrego Ubá quartzite, a number up to 120 detrital grains were randomly picked. Grains were mounted in epoxy disks and polished to expose their centers. Morphological features and internal structures of zircon grains were revealed by BSE and CL images. U-Pb (SHRIMP and LAMC-ICP-MS) analysis was performed on zircon crystals recovered from the amphibolite lenses (samples P2A and TN-8A) in order to obtain igneous crystallization and metamorphic ages. Analysis on detrital zircon grains from sample P2D (Córrego Ubá quartzite) was performed by using U-Pb (LAMC-ICP-MS) in order to determine maximum depositional ages and sedimentary provenance. The new U-Pb analyses are available in the Supplementary data file labeled as U_Pb_data.

U-Pb SHRIMP results for the amphibolite lenses (samples TN-8A and P2A)

Two amphibolite lenses were collected for geochronological U-Pb analyses: TN-8A (UTM24S: 206564E/7856556S WGS84) and P2A (UTM24S: 219363E/7841825S WGS84) (Fig. 2).

- *Sample TN-8A:* amphibolite occurring as a decimeter-thick lens, interposed in the Pocrane Complex orthogneiss. It features as a fine-grained and massive rock, composed of hornblende and plagioclase, quartz, biotite, apatite, titanite and zircon as accessory minerals. Amphibole and biotite mark the regional foliation (Sn). Twenty-four zircon grains from sample TN-8A were analyzed by

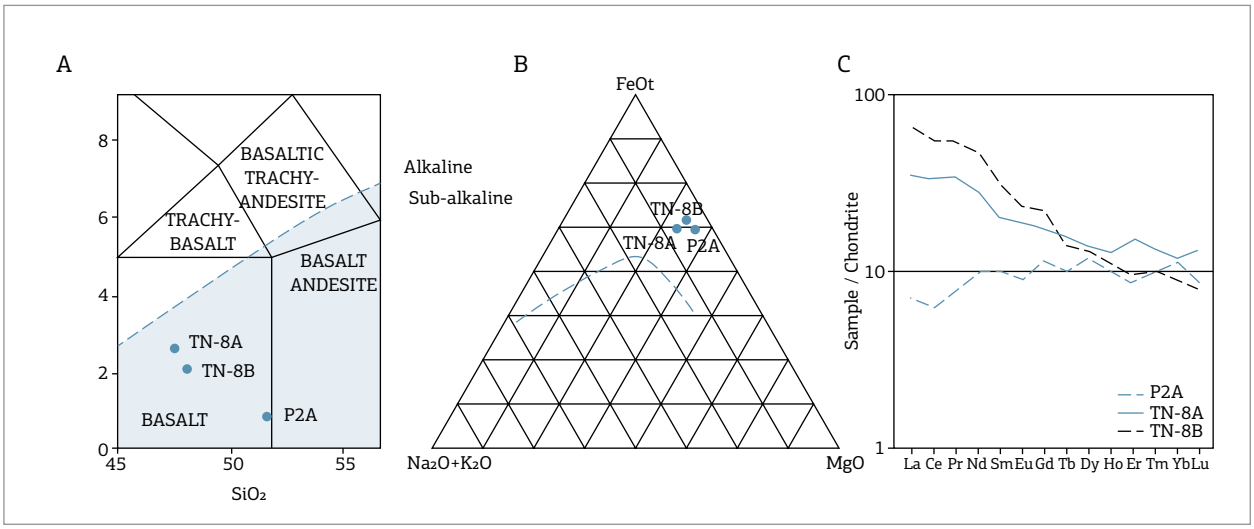

Figure 4. Classification of amphibolite samples in the diagrams: (A) TAS (Wilson 1989 and Xinhua *et al.* 2000) and alkaline and sub-alkaline diagram (Irvine & Baragar 1971 apud Rollinson 1993; (B) AFM diagram (Jensen, 1976); (C) Chondrite-normalized REE patterns (Taylor & McLennan 1985) in comparison to some general patterns — Normalized to Morb-N (Hofmann 1988), Continental Crust and Superior Crust (Weaver & Tarney 1984) and Ocean Island Basalt (OIB; Sun, 1982);

U-Pb SHRIMP. Cathodoluminescence images show two different families of zircon grains (Fig. 5A, 5B and 5C). The first one was formed by 2:1 and 3:1 ratio crystals, with preserved igneous features (e.g., 6.1 and 3.1 grains). The second family shows a prismatic proportion of 2:1 grains, with incipient to advanced metamict processes (e.g., 4.1 and 11.1 grains). Grains of the two families present a thin metamorphic overgrowth with high luminescence, which could not be dated due to the small length of its metamorphic edge. Fifteen spots with better analytical consistency result in an upper intercept age of 1,529 ± 37 Ma (MSWD = 0.25), interpreted as igneous crystallization age of TN-8A amphibolite igneous protolith (Fig. 5C). The amphibolite metamorphic age was calculated using the data from five spots with good analytical consistency, which resulted in a concordant age of 627 ± 20 Ma (MSWD = 1.6; Fig. 5A). The magmatic crystallization age and metamorphic age presented here for the TN-8A amphibolite are equal (considering the analytical errors) to the values obtained in another amphibolite lens in the nearby area (Bananal site) by Silva *et al.* (2002);

- *Sample P2A:* meter-thick boudin of amphibolite interleaved in the Pocrane Complex orthogneiss. It features a fine-grained and massive rock, but with quite a distinct foliation. It consists of amphibole, plagioclase and quartz; apatite, titanite and zircon are accessory minerals. For the P2A sample, eight

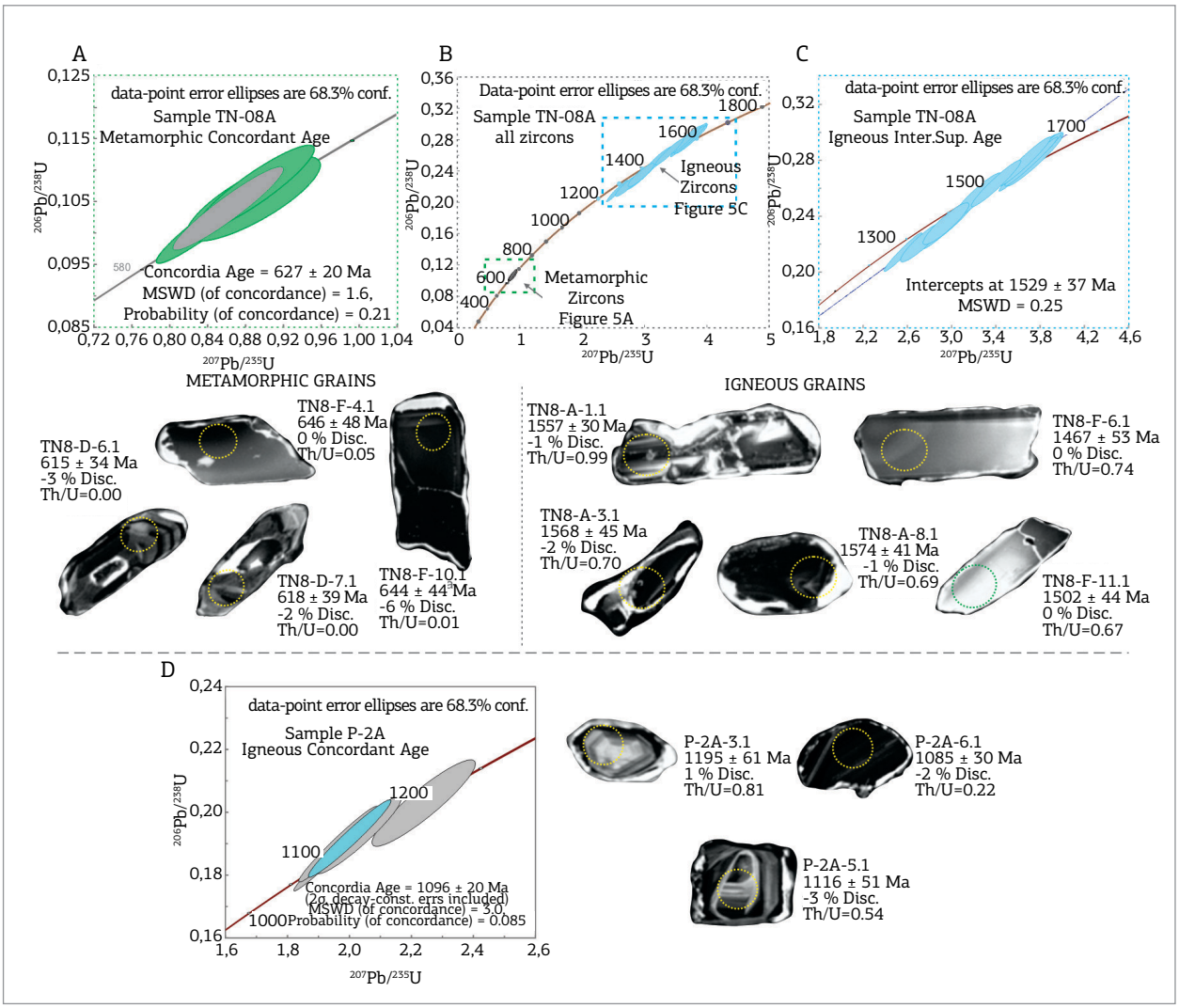

Figure 5. Ages of sample TN-8A and P2A: (A) Crystallization age of amphibolite magmatic protolith (TN-8A), given by the upper intercept Wetherill diagram, and cathodoluminescence images of analyzed grains; (B) All zircons concordia diagram of sample TN-8A; (C) Metamorphic concordant age and cathodoluminescence images of analyzed grains (spot size = 30 µm) from sample TN-8A; (D) Concordia age for igneous crystallization of P2A amphibolite protolith, and cathodoluminescence images of analyzed grain (spot size = 30 µm).

zircon grains were analyzed with U-Pb SHRIMP. CL images show zircon grains composed of equidimensional prisms, with a high luminescence metamorphic overgrowth, which cannot be analyzed due to their small size (Fig. 5D). The U and Th contents of the analyzed spots are compatible with magmatic rocks. Four measures with good analytical consistency were selected for the construction of the Wetherill diagram, which provides the concordant age of 1,096 ± 20 Ma (MSWD = 3), considering the time of igneous crystallization of the amphibolite protolith (Fig. 5D). The sample also features four inherited zircon grains, which indicate Rhyacian, Statherian and Calymmian inheritance. The Rhyacian heritage relates to the Pocrane Complex, host rock of the P2A amphibolite. The Statherian heritage relates to magmatism associated with the Juiz de Fora Complex (Duarte *et al.* 2003; Heilbron *et al.* 2010). The Calymmian heritage relates to the mafic magmatism represented by amphibolites co-genetic to sample TN-8A (this paper) and Bananal (Silva *et al.* 2002).

Detrital zircon U-Pb data

The 90 grains analyzed from sample P2D (219.592E/7.841.790N, UTM24S WGS84) — Córrego Ubá quartzite — are prismatic, short to elongated, generally showing rounded terminations and the maximum length of 300 µm. Some grains are pyramidal with a rounded core (Fig. 6). After data reduction, 87 spots could be used for age calculations. Representing 35% of analyzed zircon grains, the statistic peak around 1,176 ± 21 Ma encompasses the youngest grains of the sample (Fig. 7), which represents a younger component of the source, thus constraining the maximum depositional age of the Córrego Ubá quatzite. Furthermore, the youngest concordant grain dated shows the age of 995 ± 66 Ma. This youngest and most important population includes rounded grains and some euhedral to subhedral crystals with well-rounded shapes (Fig. 6). Other significant sources of P2A quartzite are indicated by age peaks at 1,371 ± 30 Ma (18%) and 1,536 ± 22 Ma (19%). Minor Paleoproterozoic ages point to sources around 1,803 and 1,977 Ma (Fig. 8). It is worth to mention the complete absence of Ediacaran to Ordovician sources and the lack of ages older than the Orosirian period.

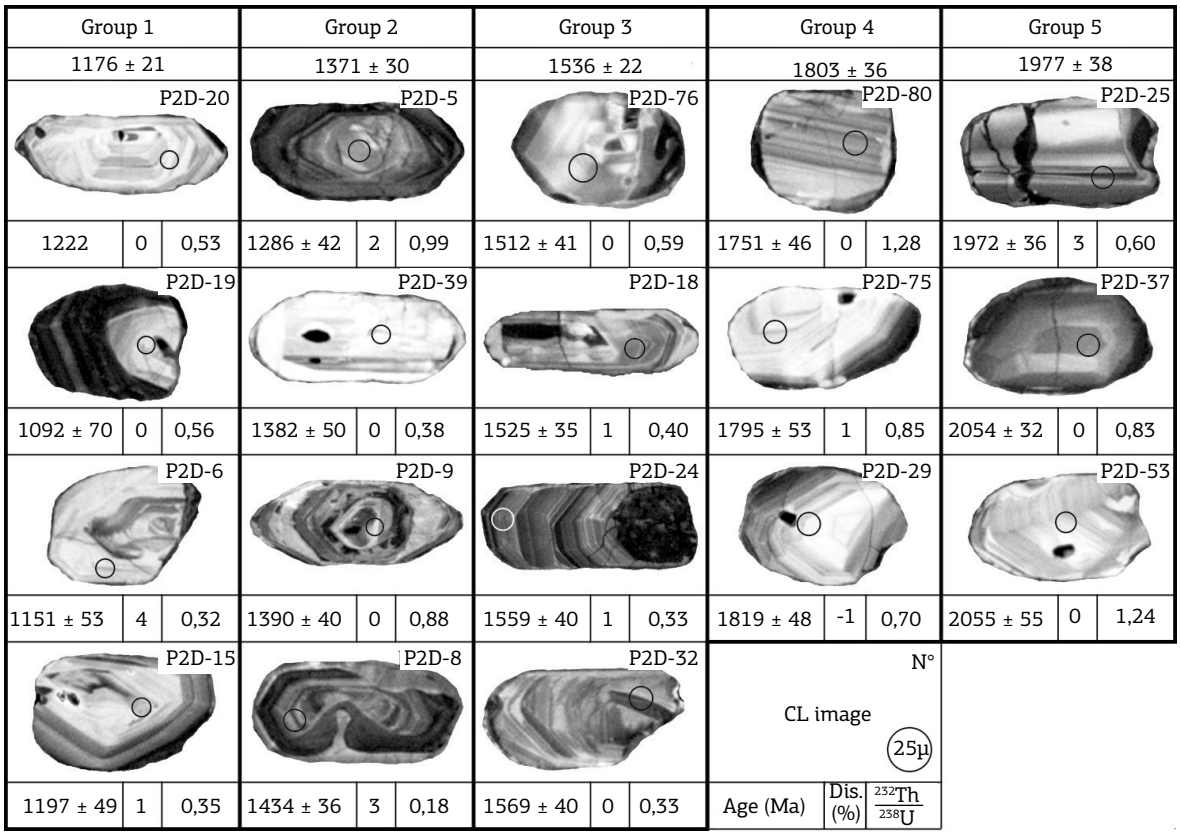

Figure 6. Cathodoluminescence (CL) images of representative zircon grains from the Córrego Ubá quartzite (sample P2D).

DISCUSSIONS

The history of the continental drift alternates long fragmentation periods with short agglutination intervals (Nance *et al.* 1988, Murphy and Nance 1992). Hence, one of the products of Rhyacian-Orosirian Orogeny would have been a paleocontinent that brought together inherited parts of the São Francisco and Congo cratons and the Araçuaí-West Congo Orogen basement (Atlantica paleocontinent; Rogers 1996, Rogers and Santosh 2004). Afterward, over a period of about 1.5 Ga (interval between the Rhyacian and Ediacaran orogenies), this paleocontinent region was spared of orogenic events with compressive nature. However, on the other hand, it experienced several tafrogenic episodes, revealed by magmatism and sedimentation periods (Pedrosa-Soares & Alkmim 2011). The new data presented in this study characterize the Córrego Ubá Quartzite and amphibolite lenses as evidence of taphrogenic events tectonically interlayered in the Pocrane Complex. These signs improve the knowledge about the Calymmian and Stenian episodes

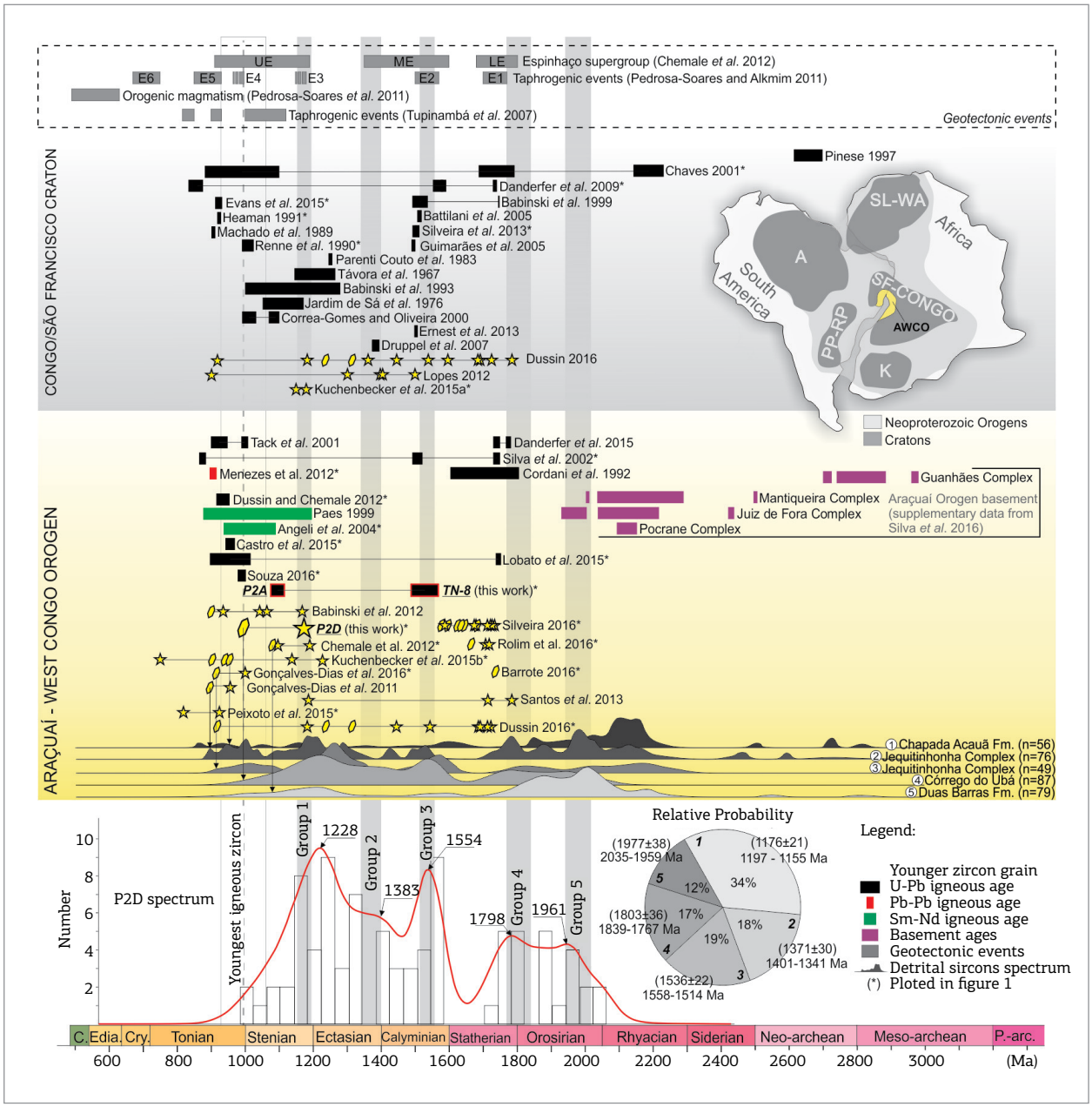

Figure 7. Ages of main extensional events in the São Francisco-Congo Craton and Araçuaí and West Congo Orogen. References: 1) Kuchenbecker *et al.* 2015a; 2) Gonçalves-Dias *et al.* 2011; 3) Gonçalves-Dias *et al.* 2016; 4) This work; 5) Chemale Jr. *et al.* 2012; Mantiqueira, Juiz de Fora and Pocrane complexes data from Silva *et al.* 2016.

as unsuccessful fragmentation attempts of São Francisco-Congo paleocontinent now described in the metamorphic, highly deformed orogenic core.

The Calymmian distensive event marks one of the oldest taphrogenic episodes ever recorded in the region of Araçuaí-West Congo Orogen (the oldest one is the Statherian event).

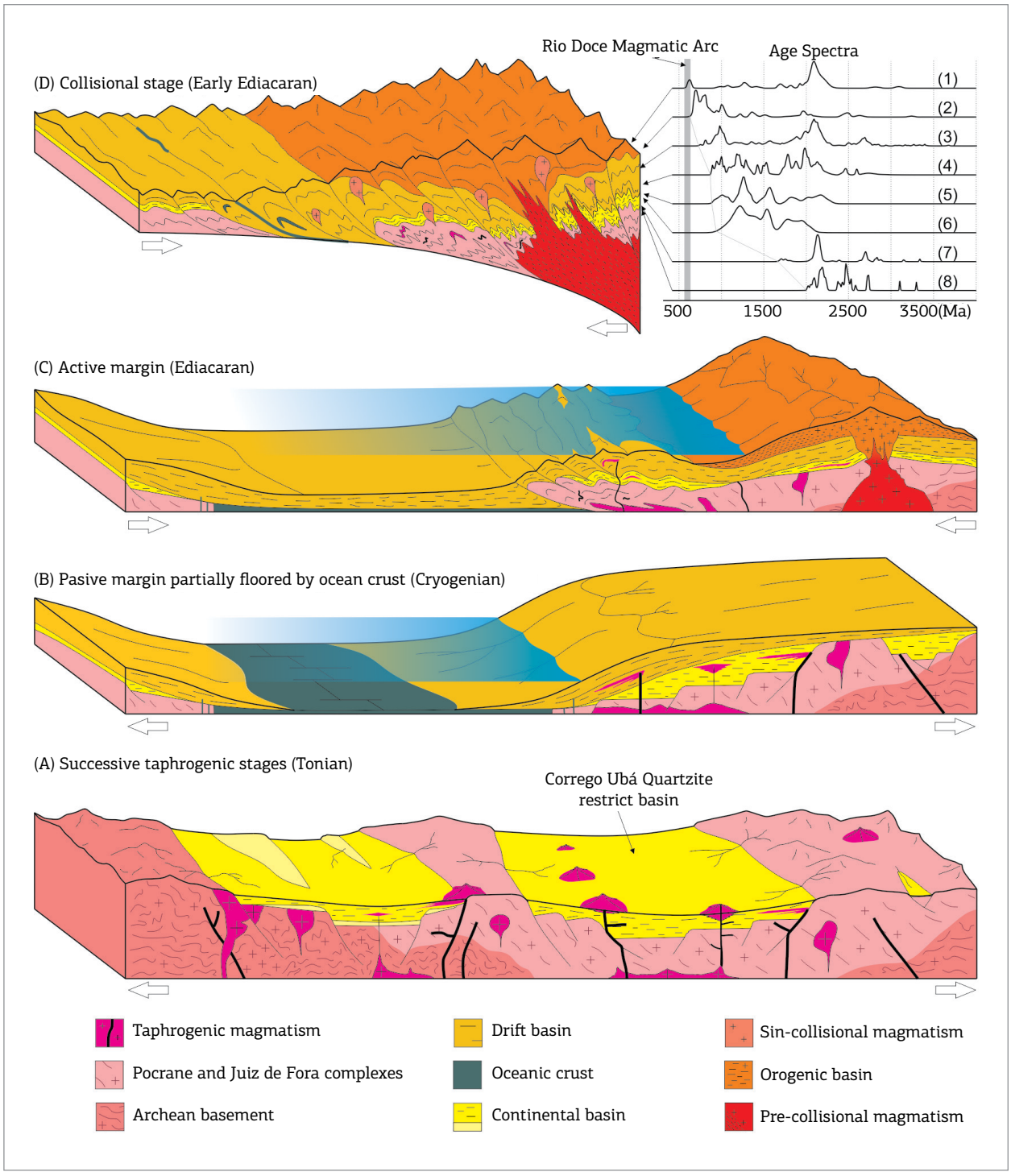

Figure 8. Tectonic model for the Mesoproterozoic-Neoproterozoic taphrogenic events and Ediacaran orogenic event in the Rio Doce Arc region, Araçuaí Orogen. 1) João Pinto Formation (Rio Doce Group), Novo 2013; 2) Palmital do Sul Formation (Rio Doce Group), Novo 2013; 3) Macaúbas Group, Kuchenbecker *et al.* 2015b; 4) Jequitinhonha Complex, Gonçalves-Dias *et al.* 2011; 5) Jequitinhonha Complex, Gonçalves-Dias *et al.* 2016; 6) This Work; 7) São João da Chapada Formation, Chemale Jr. *et al.* 2012; 8) Bandeirinhas Formation, Chemale Jr. *et al.* 2012.

Despite being regarded as part of the Espinhaço-Chapada Diamantina System (Danderfer *et al.* 2009; Babinski *et al.* 1994, 2012; Chemale Jr. *et al.* 2012; Silveira *et al.* 2013; Guadagnin *et al.* 2015), there is only one reference to this event in the Araçuaí Orogen metamorphic core (U-Pb age by Silva *et al.* 2002). The new data from this paper displays a tholeiitic composition amphibolite with crystallization age at 1,529 ± 37 Ma. Its REE pattern is similar to the basic magmatism related to continental rifting, or continental plateau basalt. These features suggest this amphibolite sample represents basic magmatism related to continental rift during Calymmian times. Reports of this approximately 1.5 Ga distensive event are common in the São Francisco-Congo Craton region (Medium Espinhaço from Chemale Jr. *et al.* 2012 and Event 2 from Pedrosa-Soares & Alkmim 2011), as well as around the globe (Bingen *et al.* 2005*,* 2008; Zhao *et al.* 2004; Ernst *et al.* 2000; Ernst *et al.* 2008; Wingate *et al.* 2009). The discovery of ca. 1.5 Ga intrusion in the reworked Araçuaí Orogen terrain is a major step to a more complete barcode record in São Francisco-Congo paleocontinent, which can be used in future paleo-continental reconstructions.

The Stenian episode is well portrayed in several studies, and thereby records a wide extension event (Tack *et al.* 2001; Tupinambá *et al.* 2007; Vicat and Pouclet 1995; Silveira *et al.* 2013). The sample P2A amphibolite from this work presents crystallization age of 1,096 ± 20 Ma and a tholeiitic gabbro composition. REE pattern correlated with advanced stage of magmatism relating to a continental rift, which confirms the tectonic environment discriminant graphics, with plots in the continental intraplate basalt fields. These features suggest the P2A amphibolite represents basic magmatism related to a Stenian continental rift. Castro *et al.* (2015) portrait similar U-Pb ages for amphibolites lenses occurred in the neighboring region. Angeli *et al.* (2004) described ultramafic rocks associated with this rift system, supporting the idea of continuous crustal thinning in the region during Stenian times. Therefore, considering this mafic-ultramafic sequence, intrusive into the continental crust, the geodynamic setting should be related to specific stages in the evolution of the São Francisco-Congo Craton.

The Córrego Ubá quartzite represents the basin formed during the abovementioned Stenian event, partially preserved in the Araçuaí-West Congo orogen metamorphic core. The U-Pb geochronology study of the Córrego Ubá quartzite provides important hints for their geotectonic and palaeogeographic interpretations. The results indicate that great part of the sedimentary supply should have come from secondary sources, located both in the São Francisco and Congo cratonic counterparts. The oldest intervals reveal contributions from Rhyacian to Stenian sources, and the absence of pre 2.05 Ga zircon grains discards São Francisco and Congo cratons basement complexes. They also require a younger source with no inheritance, which may correspond mainly to Juiz de Fora and Pocrane basement complexes from Araçuaí-West Congo Orogen (Novo, 2013; Teixeira *et al.* 2000, Silva *et al.* 2002, Barbosa & Sabaté 2004, Noce *et al.* 2007). Correspondingly, the source of this interval could also be associated to rift related granites (e.g., Borrachudos Suite). The Statherian to Cambrian peaks indicate reworked sources from Bomba Formation and Middle Espinhaço Supergroup (Danderfer *et al.* 2009, Pedrosa-Soares & Alkmim 2011, Chemale Jr. *et al.* 2012, Guadagnin *et al.* 2015). Statistical analyses point out a maximum age of deposition for the psammitic sediment, limited by 1,176 ± 21 Ma. However, the youngest concordant grain dated shows the age of 995 ± 66 Ma, suggesting the Tonian-Stenian limit.

Figure 8 shows a comparison of the detrital zircon age spectra of the Córrego Ubá quartzite, with plausible primary and secondary sources from the São Francisco-Congo Craton neighboring areas. Regardless of the lack of data from Upper Espinhaço (0.9 – 1.2 Ga; Chemale Jr. *et al.* 2012), those units show significant similitude with the Córrego Ubá quartzite spectra. Despite some differences, like the relative abundance of Archean zircon grains in the continental rift stages, units of the Upper Espinhaço, the Córrego Ubá quartzite age spectra feature great similarity to the age spectra of those units (Figs. 7 and 8A). The Córrego Ubá quartzite has no Cryogenian or Ediacaran zircons, but, instead, shows patterns that are more similar to a rift arrangement. The Córrego Ubá quartzite is then not correlative with other sedimentary successions of the Araçuaí Orogen metamorphic core (e.g., Rio Doce Group and Nova Venécia Complex – Vieira 2007, Gradim *et al.* 2014). However, instead, they probably represent a chronostratigraphic equivalent to Upper Espinhaço Basin (Chemale Jr. *et al.* 2012), an extension of the passive margin sediments formed in an intraplate setting.

Surprisingly, comparing with data from the western sector of the Araçuaí Orogen and São Francisco Craton, it is noteworthy that no igneous zircon from the three samples yielded an age older than early Orosirian (~2.05 Ga), showing age spectra essentially limited in the range of ca. 1 – 2 Ga; i.e., younger than the Late Rhyacian orogeny that amalgamated the basement, and older than the main anorogenic event (930 – 870 Ma) associated with the Early Tonian precursor basin of Araçuaí-West Congo orogen (AWCO). Therefore, it is possible to suggest that the Córrego Ubá quartzite could represent a restrict basin, confined in a juvenile basement, like the Pocrane and Juiz de Fora complexes.

During early Mesoproterozoic to late Neoproterozoic, the development of a continental rift sequence and the continued thinning of the lithosphere eventually led to plate separation and creation of a true oceanic crust (Santo

Antônio do Grama Suit; Queiroga *et al.* 2006, 2007, Fig. 8B), extending to ca. 660 Ma. This basin evolved from a continental rift system surrounded by the São Francisco-Congo Paleocontinent, to an inland-sea basin (a gulf), partially floored by ocean crust (Pedrosa-Soares *et al.* 2011; Alkmim *et al.* 2006; Queiroga *et al.* 2007; Peixoto *et al.* 2015). In the Ediacaran Period, the pre-collisional Rio Doce magmatic arc marked the onset of a subduction-related convergent stage, followed by regional deformation and metamorphism in the collisional stage, that provided intense tectonism, basin inversion and obduction of oceanic crust slices (Queiroga *et al.* 2006, 2007; Tupinamba *et al.* 2007, Figs. 8C and 8D).

From a global tectonic standpoint, the Córrego Ubá quartzite and the mafic intrusives of the Pocrane Complex might be correlated to the extensional processes that led to the fragmentation of a supercontinent (Atlantica). It could also mark the dismembering of the São Francisco-Congo Paleocontinent, which was later amalgamated with other blocks in the Gondwana Supercontinent during the Brasiliano/Pan-African Orogeny (Tedeschi *et al.* 2015; Gonçalves *et al.* 2015; Pedrosa-Soares *et al.* 1998, 2007; Alkmim *et al.* 2006, 2007; Brito Neves & Sato 2001; Tack *et al.* 2001; Vicat & Pouclet 1995).

CONCLUSION

The mafic intrusions from southeastern Brazil characterize important regional geological events in the São Francisco-Congo Craton and its surrounding Neoproterozoic mobile belts. The amphibolite lenses are interpreted as mafic intrusions, related to the Calymmian and Stenian rifting stages. They might also be correlated to the extensional events that led to the break-up and dispersion of a Paleoproterozoic supercontinent, and thus relate to the mafic dike swarms and other intrusions throughout the São Francisco-Congo paleocontinent and surrounding areas (Figs. 1, 7 and 8A). The intrusions infer continued lithospheric thinning with associated volcanism. The amphibolite lenses, thus, provide a benchmark for the onset of the Calymmian and Stenian continental rifting in this area, and set an important marker for the registration of the Atlantica breakup and dispersion processes in South America.

The Córrego Ubá quartzite shows detrital zircon U-Pb age spectra, indicating sources limited in the range of ca. 1 – 2 Ga, with complete absence of Cryogenian-Ediacaran peak, excluding sources related to the Brasiliano cycle. Therefore, it cannot be associated to other metasediment units of the Araçuaí Orogen metamorphic core, like Rio Doce Group. Additionally, the detrital zircon age spectra of the Córrego Ubá quartzite displays great similarity to continental rift related units. Thus, it represents one of the several unsuccessful fragmentation attempts of São Francisco-Congo paleocontinent, deposited in a restrict basin, probably during Stenian times. It can be associated with the Tonian extensional tectonism at the São Francisco-Congo Craton area. This is the first time that such kind of basin is described in Araçuaí-West Congo Orogen reworked metamorphic core.

All together, these continental taphrogenic events testify the several unsuccessful fragmentation attempts that affected the long-lived São Francisco-Congo Palaeocontinent, which remained preserved from a complete break-up associated with ocean spreading from the Early Orosirian to the Atlantic opening in Cretaceous time.

ACKNOWLEDGEMENTS

The authors are grateful to the Brazilian research and development agencies (CNPq, CAPES, CODEMIG, CPRM, Petrobras) for financial support, and to technical staffs of the geochronological laboratories of São Paulo University, for isotopic analyses.

REFERENCES

Alkmim F.F., Pedrosa-Soares A.C., Noce C.M., Cruz S.C.P. 2007. Sobre a Evolução Tectônica do Orógeno Araçuaí-Congo Ocidental. *Geonomos*, **15**:25-43.

Alkmim F.F., Marshak S., Pedrosa-Soares A.C., Peres G.G., Cruz S.C.P., Whittington A. 2006. Kinematic evolution of the Araçuaí–West Congo orogen in Brazil and Africa: Nutcracker tectonics during the Neoproterozoic assembly of Gondwana. *Precambrian Research*, **149**:43-63.

Angeli N., Teixeira W., Heaman L., Fleet M.E., Moore M., Sato K. 2004. Geochronology of the Ipanema Layered Mafic-Ultramafic Complex, Minas Gerais, Brazil: evidence of extension at the Meso-Neoproterozoic time boundary. *International Geology Review*, **46**(8):730-744.

Babinski M., Pedrosa-Soares A.C., Trindade R.I.F., Martins M., Noce C.M., Liu D. 2012. Neoproterozoic glacial deposits from the Araçuaí orogen, Brazil: Age, provenance and correlations with the São Francisco craton and West Congo belt. *Gondwana Research*, **21**:451-465.

Babinski M., Pedreira A., Brito-Neves B.B., Van Schmus W.R. 1999. Contribuição à geocronologia da Chapada Diamantina. In: SBG, 7º Simpósio Nacacional Estudos Tectônicos, *Anais*, p. 118-120.

Babinski M., Brito-Neves B.B., Machado N., Noce C.M., Uhlein A., Van Schmus W.R. 1994. Problemas da Metodologia U-Pb com Zircões de Vulcânicas Continentais: Caso do Grupo Rio dos Remédios, Supergrupo Espinhaço, no Estado da Bahia. In: SBG, 38º Congresso Brasileiro de Geologia, *Anais*, v. 2, p. 409-410.

Babinski M., Van Schmus W.R., Chemale Jr. F., Brito Neves B.B., Rocha A.J.D. 1993. Idade isocrônica Pb/Pb em rochas carbonáticas da Formação Caboclo, em Morro do Chapéu, BA. 2º Simpósio sobre o Cráton do São Francisco, Salvador, *Anais*, p. 160-163.

Barbosa J.S.F. & Sabaté P. 2004. Archean and Paleoproterozoic crust of the São Francisco Craton, Bahia, Brazil: geodynamic features. *Precambrian Research*, **133**:1-27.

Battilani G.A., Vasconcelos P.M., Gomes N.S., Guerra W.J. 2005. Geochronological data of dykes and sills intruding Proterozoic sequences of the Tombador Formation, Bahia — Brazil. 3º Simpósio do Cráton do São Francisco, Salvador, *Short Papers*, v. 1, p. 139-142.

Barrote V.R. 2016. *A sequencia Portadora de Formações ferríferas de Guanhães, Minas Gerais, Brasil*. MS Dissertation, Instituto de Geociências, Universidade Federal de Minas Gerais, Belo Horizonte, 103 p.

Bingen B., Andersson J., Söderlund U., Möller C. 2008. The Mesoproterozoic in the Nordic countries. *Episodes*, **31**(1):1-6.

Bingen B., Skar O., Marker M., Sigmond E.M.O., Nordgulen O., Ragnhildstveit J., Mansfeld J., Tucker R.D., Liégeois J.P. 2005. Timing of continental building in the Sveconorwegian orogen, SW Scandinavia. *Norwegian Journal of Geology*, **85**:87-116.

Black L.P., Kamo, S.L., Allen C.M., Aleinikoff J.N., Davis D.W., Korsch R.J., Foudoulis C. 2003. TEMORA 1: a new zircon standard for Phanerozoic U-Pb geochronology. *Chemical Geology*, **200**:155-170.

Brito Neves B.B. & Sato K. 2001. Marcos cronogeológicos da evolução do embasamento pré-Ordoviciano da Plataforma Sul-Americana-avaliação para o final do ano 2000. *Estudos Geológicos-Série B Estudos e Pesquisas*, Recife-UFPE, **11**:1-25.

Castro M.P., Queiroga G., Martins M., Pedrosa-Soares A.C., Dussin I., Alkmim F. 2015. A Formação Capelinha e seu magmatismo: registro de uma das primeiras tentativas de quebra do Paleocontinente São Francisco-Congo no Orógeno Araçuaí. 15º Simpósio Nacional de Estudos Tectônicos - IX International Symposium on Tectonics.

Cawood P.A., Hawkesworth C.J., Dhuime B. 2012. Detrital zircon record and tectonic setting. *Geology*, **40**(10):875-878.

Chaves A.O. 2001. *Enxames de diques máficos do setor sul do Cráton do São Francisco (MG, Brasil)*. PhD Thesis, Instituto de Geociências, Universidade de São Paulo, São Paulo,153 p.

Chemale Jr. F., Dussin I., Alkmim F., Martins M.S., Queiroga G., Armstrong R., Santos M. 2012. Unravelling a Proterozoic basin history through detrital zircon geochronology: The case of the Espinhaço Supergroup, Minas Gerais, Brazil. *Gondwana Research*, **22**:200-206.

Cordani U.G., Iyer S.S., Taylor P.N., Kawashita K., Sato K., McReath I. 1992. Pb-Pb, Rb-Sr, and K-Ar systematic of the Lagoa Real uranium province (south-central Bahia, Brazil) and the espinhaço Cycle (ca. 1.5-1.0 Ga). *Journal of South American earth Sciences*, **1**:33-46.

Correa Gomes L.C. and Oliveira E.P. 2000. Radiating 1.0 Ga mafic dyke swarms of eastern Brazil and western Africa: evidence of post-assembly extension in the Rodinia supercontinent?. *Gondwana Research*, **3**(3):325-332.

Danderfer A., Lana C.C., Nalini Jr. H.A., Costa A.F.O. 2015. Constraints on the sthatherian Evolution of the intraplate rifting in a Paleo-Mesoproterozoic paleocontinent: New stratigraphic and geochronology record from the eastern São Francisco craton. *Gondwana Research*, **28**:668-688.

Danderfer A., Waele B., Pedreira A.J., Nalini H.A. 2009. New geochronological constraints on the geological evolution of Espinhaço basin within the São Francisco Craton Brazil. *Precambrian Research*, **170**:116-128.

Drüppel K., Littmann S., Romer R.L., Okrusch M. 2007. Petrology and isotopic geochemistry of the Mesoproterozoic anorthosite and related rocks of the Kunene Intrusive Complex, NW Namibia. *Precambrian Research*, **156**:1-31.

Duarte B.P., Heilbron M., Valladares C., Nogueira J.R., Tupinambá M., Eirado L.G., Almeida J.C., Almeida G.C. 2003. *Geologia das Folhas Juiz de Fora e Chiador*. In: A.C. Pedrosa Soares, C.M. Noce, R. Trouw, M. Heilbron (coord.). Projeto Sul de Minas, Belo Horizonte, COMIG/SEME, v. 1, cap. 6, p. 153-258.

Dussin I.A. 2016 Geocronologia U-Pb e Lu-Hf, em zircão detrítico, aplicada a uma bacia proterozoica. exemplo: evolução sedimentar e tectônica da bacia espinhaço – setor meridional-MG. Thesis. Universidade Estadual do Rio de Janeiro, 117p.

Dussin I.A. & Chemale F. Jr. 2012. *Geologia Estrutural e Estratigrafia do Sistema Espinhaço-Chapada Diamantina e sua aplicação nas Bacias Mezocenozóicas da Margem Passiva Brasileira*, 1, Belo Horizonte, Particular, 218 p.

Ernest R.E., Pereira E., Hamilton M.A., Pisarevsky S.A., Rodrigues J., Tassinari C.C.G., Teixeira W., Van-Dunem V. 2013. Mesoproterozoic intraplate magmatic 'barcode' record of the Angola portion of the Congo Craton: Newly dated magmatic events at 1505 and 1110 Ma and implications for Nuna (Columbia) supercontinent reconstructions. *Precambrian Research*, **230**:103-118.

Ernest R.E., Buchan K.L., Hamilton M.A., Okrugin A.V., Tomshin M.D. 2000. Integrated paleomagnetism and U–Pb geochronology of mafic dikes of the Eastern Anabar Shield Region, Siberia: implications for the Mesoproterozoic paleolatitude of Siberia and comparison with Laurentia. *Journal of Geology*, **108**:381-401.

Evans D.A.D., Trindade R.I.F., Catelani E.L., D'agrella-Filho M.S., Heaman L.M., Oliveira E.P., Soderlund U., Ernest R.E., Smirnov A.V., Salminen J.M. 2015 Return to Rodinia? Moderate to high palaeolatitude of the São Fnacisco/Congo craton at 920 Ma. In: Supercontinent Cycles Through Earth History Geological Society, London, Sepecial Publications, 424 p.

Féboli & Paes 2000. Projeto Leste-MG. Folha Itanhomi (SE.24-Y-C-I), Belo Horizonte, SEME/COMIG/CPRM, escala 1:100.000.

Gonçalves L., Alkmim F., Pedrosa-Soares A.C., Dussin I.A., Valeriano C.M., Lana C., Tedeschi M.F., 2015. Granites of the intracontinental termination of a magmatic arc: an example from the Ediacaran Araçuaí Orogen, Southeastern Brazil. *Gondwana Res.*, **36**:439-458.

Gonçalves-Dias T., Caxito F., Pedrosa-Soares A., Stevenson R., Dussin D., Silva L.C., Alkmim F., Pimentel M., 2016. Age, provenance and tectonic setting of the high-grade Jequitinhonha Complex, Araçuaí Orogen, eastern Brazil. *Brazilian Journal of Geology*, **46**(2):199-219.

Gonçalves-Dias T., Pedrosa-Soares A.C., Dussin I.A., Alkmim F.F., Caxito F.A., Silva L.C., Noce C.M. 2011. Idade máxima de sedimentação e proveniência do Complexo Jequitinhonha na áreatipo (Orógeno Araçuaí): primeiros dados U–Pb (LA-ICP-MS) de grãos detríticos de zircão. *Geonomos*, **19**(2):121-130.

Gradim C., Roncato J., Pedrosa-Soares A.C., Cordani U., Dussin I., Alkmim F., Queriroga G., Jacobsohn T., Silva L.C., Babinski M. 2014. The hot back-arc zone of the Araçuaí orogen, Eastern Brazil: from sedimentation to granite generation. *Brazilian Journal of Geology.*, **44**:155e180.

Guadagnin F., Chemale Jr. F., Magalhães J., Santana A., Dussin I., Takehara L. 2015. Age constraints on crystal-tuff from the Espinhaço supergroup - insight into the Paleoproterozoic to Mesoproterozoic intracratonic basin cycles of the Congo-São Francisco Craton. *Gondwana Res.*, **27**:363-376.

Guimarães J.T., Teixeira L.R., Silva M.G., Martins A.A.M., Filho E.L.A., Loureiro H.S.C. Arcanjo, J.B., Souza J.D., Neves J.P., Mascarenhas J.F., Melo R.C., Bento,R.V. 2005. Datações U–Pb em rochas magmáticas intrusivas no Complexo Paramirim e no Rifte Espinhaço: uma contribuição ao estudo da evolução geocronológica da Chapada Diamantina. 3º Simpósio sobre o Cráton do São Francisco, *Short Papers*, Salvador, pp. 159-161.

Heaman L. 1991. U-Pb dating of giant radiating dyke swarms: potential for global correlation of mafic events. In: Intern. Symp. on mafic dykes, São Paulo, *Ext. Abst*., p. 7-9.

Heilbron M., Duarte B., Valeriano C., Simonetti A., Machado N., Nogueira J. 2010. Evolution of reworked Paleoproterozoic basement rocks within the Ribeira belt (Neoproterozoic), SE-Brazil, based on U Pb geochronology: Implications for paleogeographic reconstructions of the São Francisco-Congo paleocontinent. *Precambrian Research*, **178**:136-148.

Hofmann A.W. 1988. Chemical differentiation of the Earth: the relationship between mantle, continental crust, and oceanic crust. *Earth and Planetary Science Letters,* **90**:297-314.

Jardim de Sá E.F., McReath I., Brito Neves B.B., Bartels R.L. 1976. Novos dados geocronológicos sobre o Craton São Francisco no Estado da Bahia. Anais, 29º Congresso Brasileiro de Geologia, Ouro Preto, *Anais*, v. 4, p. 185-204.

Jensen L.S. 1976. A new cation plot for classifying subalkalic volcanic rocks. Ontario Div. Mines. Misc. Pap. 66.

Klötzli U., Klötzli E., Günes Z., Košler J. 2009. Accuracy of Laser Ablation U-Pb Zircon Dating: Results from a Test Using Five Different Reference Zircons. Geostandards And *Geoanalytical Research*, **33**:5-15.

Kuchenbecker M., Reis H.L.S., Silva. L.C., Costa R.D., Fragoso D.G.C., Knauer L.G., Dussin I.A., Pedrosa-Soares A.C. 2015a. Age constraints for deposition and sedimentary provenance of Espinhaço Supergroup and Bambuí group in eastern São Francisco craton, *Geonomos*, **23(2)**:14-28.

Kuchenbecker M., Pedrosa-Soares A.C., Babinski M., Fanning M. 2015b. Detrital zircon age patterns and provenance assessment for pre-glacial to post-glacial successions of the Neoproterozoic Macaúbas Group, Araçuaí orogen, Brazil. *Precambrian Research*, **266**:12-26.

Lobato L.M., Pimentel M.M., Cruz S.C.P., Machado N., Noce C.M., Alkmim F.F. 2015. U-Pb geochronology of the Lagoa Real uranium district, Brazil: Implications for the age of the uranium mineralization. *Journal of South American Earth Sciences*, **58**:129-140.

Lopes T.C. 2012. O Supergrupo Espinhaço na Serra do Cabral, Minas Gerais: contribuição ao estudo de proveniência sedimentar. MS Dissertation, Instituto de Geociências, Universidade Federal de Minas Gerias, Belo Horizonte, 115 p.

Ludwig K.R. 2003. Using Isoplot/Ex, Version 3.00, a Geochronological Tool Kit for Microsoft Excel. Berkeley Geochronology Center. Special Publication, v. 1, p.43.

Machado N., Schrank, A., Abreu, F.R., Knauer, L.G., Almeida-Abreu, P.A., 1989. Resultados preliminares da geocronolgia U/Pb na Serra do Espinhaço Meridional. 5º Simp. Geol. Minas Gerais, Belo Horizonte, *Anais*, 171-174 p.

Menezes R.C.L., Conceição H., Rosa M.L.S., Macambira M.J.B., Galarza M.A., Rios D.C. 2012. Geoquímica e geocronologia de granitos anorogênicos tonianos (ca. 914-899 Ma) da Faixa Araçuaí no sul do estado da Bahia. *Geonomos*, **20**(1):1-13.

Murphy J.B., Nance R.D. 1992. Mountain belts and the supercontinent cycle. *Scientific American*, **266**(4):84-91.

Nance R.D., Worsley T., Moody J.B. 1988. The supercontinent cycle. *Scientific American*, **25**(1):72-79.

Noce C.M., Pedrosa-Soares A.C., Silva L.C., Armstrong R., Piuzana D., 2007. Evolution of polyciclic basement complexes in the Araçuaí orogen, based on U–Pb SHRIMP data: Implications for Brazil–Africa links in Paleoproterozoic time. *Precambrian Research*, **159**:60-78.

Novo T. 2013. *Caracterização do Complexo Pocrane, magmatismo básico mesoproterozóico e unidades neoproterozóicas do sistema Araçuaí–Ribeira, com ênfase em geocronologia U-Pb (SHRIMP e LA–ICP–MS)*. PhD Thesis, Instituto de Geociências, Universidade Federal de Minas Gerais, Belo Horizonte, 193p.

Novo T., Pedrosa-Soares A.C., Noce C.M., Alkmim F.F., Dussin I. 2010. Rochas charnockíticas do sudeste de Minas Gerais: a raiz granulítica do arco Magmático do Orógeno Araçuaí. *Revista Brasileira de Geociências*, **40**(4):573-592.

Oliveira M.J.R. 2000. Projeto Leste-MG. Folha Conselheiro Pena (SE.24-Y-C-II), Belo Horizonte, SEME/COMIG/CPRM, escala 1:100.000.

Paes V. 1999. *Geologia e geoquimica de rochas metamaficas e meta-ultramaficas da região de Alvarenga-MG e suas implicações geotectônicas*. MS Dissertation, Instituto de Geociências, Universidade Federal de Minas Gerais, Belo Horizonte, 173p.

Parenti Couto J.G., Teixeira W., Cordani U.G. 1983. Considerações sobre as principais épocas de fraturamento do Craton do São Francisco, com base em datações K–Ar em rochas básicas, II Simpósio Geologia MG, Belo Horizonte, *Anais*, p. 38-49.

Pedrosa-Soares A.C., and Alkmim F.F. 2011. How many rifting events preceded the development of the Araçuaí-West Congo orogen? *Geonomos*, **19**(2):244-251.

Pedrosa-Soares A.C., Campos C.P., Noce C., Silva, L.C., Novo T., Roncato J., Medeiros S., Castañeda C., Queiroga G., Dantas E., Dussin I., Alkmim F.F. 2011. Late Neoproterozoic-Cambrian granitic magmatism in the Araçuaí orogen (Brazil), the Eastern Brazilian Pegmatite Province and related mineral resources. In: Sial A.N., Bettencourt J.S., De Campos C.P., Ferreira V.P. (eds). *Granite-Related Ore Deposits*. Geological Society, London, Special Publications, **350**:25-51.

Pedrosa-Soares A.C., Alkmim F.F., Tack L., Noce C.M., Babinski M., Silva L.C., Martins-Neto M.A. 2008. Similarities and differences between the Brazilian and African counterparts of Neoproterozoic Araçuaí-West Congo orogen. In: Pankhrust R., Trouw R., Brito-Neves B B., Wit M. (eds). The Gondwana Peleocontinent in the South Atlantic Region. *Geological Society of London, Special Publications*, **294**:153-172.

Pedrosa-Soares A.C., Noce C.M., Alkmim F.F., Silva L.C., Babinski M., Cordani U. Castañeda C. 2007. Orógeno Araçuaí: Síntese do Conhecimento 30 anos após Almeida 1977. *Geonomos*, **15**(1):1-16.

Pedrosa-Soares A.C., Noce C.M., Wiedemann C.M., Pinto C.P. 2001. The Araçuaí–West Congo orogen in Brazil: An overview of a confined orogen formed during Gondwanland assembly. *Precambrian Research*, **110**:307-323.

Pedrosa-Soares A.C., Vidal P., Leonardos O.H., Brito-Neves B.B. 1998. Neoproterozoic oceanic remnants in eastern Brazil: Further evidence and refutation of an exclusively ensialic evolution for the Araçuaí-West Congo Orogen. *Geology*, **26**(6):519-522.

Peixoto E.N., Pedrosa-Soares A.C., Alkmim F.F., Dussin I.A. 2015. A suture-related accretionary wedge formed in the Neoproterozoic Araçuaí orogen (SE Brazil) during Western Gondwanaland assembly. *Gondwana Research*, **27**:878-896.

Pinese J.P.P. 1997. *Geologia, geoquímica isotópica e aspectos dos diques máficos pré-cambrianos da região de Lavras (MG), porção sul do Cráton do São Francisco*. PhD Thesis, Instituto de Geociências, Universidade de São Paulo, São Paulo, 178 p.

Queiroga G.N., Pedrosa-Soares A.C., Noce C.M., Alkmim F.F., Pimentel M.M., Dantas E., Martins M., Castañeda C., Suita M.T.F., Prichard H. 2007. Age of the Ribeirão da Folha ophiolite, Araçuaí Orogen: The U-Pb zircon dating of a plagiogranite. *Geonomos*, **15**:61-65.

Queiroga G.N., Pedrosa-Soares A.C., Quemeneur J., Castañeda C. 2006. A Unidade metasedimentar do ofiolito de Ribeirão da Folha, Orógeno Araçuaí, Minas Gerais: petrografia, geotermobarometria e calcografia. *Geonomos*, **14**:25-35.

Renne P.R., Onstott T.C., D'Agrella-Filho M.S., Pacca I.G., Teixeira W. 1990.^{40}Ar/^{39}Ar dating of 1.0–1.1 Ga magnetizations from the São Francisco and Kala-hari Cratons: tectonic implications for Pan-African and Brasiliano mobile belts. *Earth and Planetary Science Letters*, **101**:349–366.

Rogers J.W., Santosh M. 2004. *Continents and Supercontinents*. Oxford University Press, 289 p.

Rogers J.J.W. 1996. A history of continents in the past three billion years. *Journal of Geology* **104**(1):91–107.

Rolim V.K., Rosière C.A., Santos J.O.S., Mcnaughton N.J. 2016. The Orosirian-Statherian banded iron formation-bearing sequences of Southern border of the Espinhaço Range, Southeast Brazil. *Journal of South American Earth Sciences*, **65**:43-66.

Rollinson H.R. 1993. *Using Geochemical Data: Evaluation, Presentation, Interpretation*, Longman 352 pp.

Santos M.N., Chemale Jr. F., Dussin I.A., Martins M., Assis T.A.R., Jelinek A.R., Guadagnin F., Armstrong R. 2013. Sedimentological and paleoenvironmental constraints of the Statherian and Stenian Espinhaço rift system, Brazil. *Sedimentary Geology*, **290**:47-59.

Silva L.C., Pedrosa-Soares A.C., Armstrong R., Pinto C.P., Magalhães J.T.R., Pinheiro M.A.P., Santos G.G. 2016. Disclosing the Paleoarchean to Ediacaran history of the Sao Francisco craton basement: The Porteirinha domain (northern Araçuaí orogen, Brazil). *Journal of South American Earth Sciences*, **68**:50-67.

Silva L.C., Armstrong R., Noce C.M., Carneiro M., Pimentel M.M., Pedrosa-Soares A.C., Leite C., Vieira V.S., Silva M., Paes V., Cardoso Filho J. 2002. Reavaliação da evolução geológica em terrenos pré-cambrianos brasileiros com base em novos dados U-Pb SHRIMP, parte II: Orógeno Araçuaí, Cinturão Móvel Mineiro e Cráton São Francisco Meridional. *Revista Brasileira de Geociências* **32**:513-528.

Silva J.M.R, Lima M.I.C., Veronese V.F., Ribeiro Junior R.N., Siga-Júnior O. 1987. Geologia, Folha SE.24 Rio Doce. Rio de Janeiro, IBGE, Projeto Radambrasil, Levantamento de Recursos Naturais, v. 34.

Silveira E.M., Söderlund U., Oliveira E.P., Ernst R.E., Menezes Leal A.B. 2013. First precise U–Pb baddeleyite ages of 1500 Ma mafic dykes from the São Francisco Craton, Brazil, and tectonic implications. *Lithos*, **174**:144-156.

Silveira V.D. 2016. *Geologia e Geocronologia de zircões detríticos da região de Serro, Serra do Espinhaço Meridional, Minas Gerais, Brasil*. MS Dissertation, Instituto de Geociências, Universidade Federal de Minas Gerais, Belo Horizonte, 112 p.

Sláma J., Košler J., Condon D.J., Crowley J.L., Gerdes A., Hanchar J.M., Horstwood M.S.A., Morris G.A., Nasdala L., Norberg N., Schaltegger U., Schoene B., Tubrett M.N., Whitehouse M.J. 2008. Plešovice zircon – a new natural reference material for U–Pb and Hf isotopic microanalysis. *Chemical Geology*, **249**:1-35.

Souza M.E.S. 2016. *Caracterização Litoestrutural e Geocronológica dos Xistos Verdes e Metagabros do Grupo Macaúbas na Faixa Terra Branca - Planalto de Minas, Minas Gerais*. MS Dissertation, Departamento de Geologia, Universidade Federal de Ouro Preto, Ouro Preto, 151 p.

Sun S.S. 1982. Chemical composition and the origin of the earth primitive mantle. *Geochimica et Cosmochimica Acta*, **46**:179-192.

Tack L., Wingate M.T.D., Liégeois J.P., Fernandez-Alonso M., Deblond A. 2001. Early Neoproterozoic magmatism (1000-910 Ma) of the Zadinian and Mayumbian groups (Bas-Congo): Onset of Rodinian rifting at the western edge of the Congo craton. *Precambrian Research*, **110**:277-306.

Távora F.I., Cordani U.G., Kawashita K. 1967. Determinações de idade potássioargônio em rochas da região central da Bahia. In: 21º Congresso Brasileiro de Geologia, Sociedade Brasileira de Geologia, Curitiba, *Anais*, p. 214–224.

Taylor S.R. and McLennan S.M. 1985. *The Continental Crust: Its Composition and Evolution*. Blackwell, Scientific Publication, Carlton, 312 p.

Tedeschi M., Novo T., Pedrosa-Soares A.C., Dussin I., Tassinari C., Silva L.C., Gonçalves L., Alkmim F.F., Lana C., Figueiredo C., Dantas E., Medeiros S., De Campos C., Corrales F., Heilbron M. 2015. The Ediacaran Rio Doce magmatic arc revisited (Araçuaí-Ribeira orogenic system, SE Brazil). *Journal of South American Earth Sciences*, **68**:167-186.

Teixeira W., Sabaté P., Barbosa J.S.F., Noce C.M., Carneiro M.A. 2000. Archean and Paleoproterozoic Tectonic evolution of the São Francisco Craton, Brazil. In: Cordani U.G., Milani E.J., Thomas Filho A., Campos D.A. (eds.). Tectonic Evolution of the South America. 31º International Geological Congress, Rio de Janeiro, Brazil, p. 101-137.

Tuller, M. 2000. Projeto Leste-MG. Folha Ipanema (SE.24-Y-C-IV), Belo Horizonte, SEME/COMIG/CPRM, escala 1:100.000.

Tupinambá M., Machado, N., Heilbron M., Ragatky C.D. 2007. Meso-neoproterozoic lithospheric extensional events in the São Francisco Craton and its surrounding south American and African metamorphic belts: a compilation of U-Pb ages. *Revista Brasileira de Geociências*, **37**:87-91.

Van Achterbergh, E., Ryan, C.G., Jackson, S.E., Griffin, W., 2001. Data reduction software for LA-ICP-MS. In: Sylvester, P. (Ed.), Laser Ablation ICPMS in the Earth Science. *Mineralogical Association of Canada*, **29**:239-243.

Vicat J.P. and Pouclet A. 1995. Nature du magmatisme lie a une extension prePanafricaine: les dolerites des bassins de Comba et de Sembe-Ouesso (Congo). *Bulletin de la Société Géologique de France*. **166**:355-364.

Vieira V.S. 2007. Significado do Grupo Rio Doce no Contexto do Orógeno Araçuaí. Ph.D. thesis, Universidade Federal de Minas Gerais, Belo Horizonte, 177 p.

Weaver B.L. and Tarney J. 1984. Empirical approach to estimating the composition of the continental crust. *Nature*, **310**:575-577.

Wilson M. 1989. Igneous Petrogenesis. London: Unwin Hyman, 470p.

Wingate M.T.D., Pisarevsky S.A., Gladkochub D.P., Donskaya T.V., Konstantinov K.M., Mazukabzov A.M., Stanevich A.M. 2009. Geochronology and paleomagnetism of mafic igneous rocks in the Olenek Uplift, northern Siberia: Implications for Mesoproterozoic supercontinents and paleogeography. *Precambrian Research*, **170**:256-266.

Xinhua Z., Yin A. and Ryerson F.J. 2000. The Zedong Window: A record of superposed Tertiary convergence in southeastern Tibet. *Journal of Geophysical Research*, **105**:19.211-19.230.

Zhao G., Sun M., Wilde S.A., Li S. 2004. A Paleo-Mesoproterozoic supercontinent: assembly, growth and breakup. *Earth-Science Reviews*, **67**:91-123.

APPENDIX

Data available in the Supplementary data file labeled as Lithochemical_Data
Lythochemical analysis of amphibolite samples (major elements in % weight; trace in ppm).

SAMPLE	P2A	TN-8A	TN-8B
SiO_2	51.57	47.43	47.97
TiO_2	0.99	1.71	2.81
Al_2O_3	16.04	16.6	15.61
Fe_2O_3	11.8	14.31	15.43
MnO	0.13	0.2	0.17
MgO	6.06	5.83	6.59
CaO	11.64	10.02	7.91
Na_2O	0.67	2.01	1.37
K_2O	0.18	0.67	0.7
P_2O_5	0.06	0.35	0.41
LOI	0.6	0.6	0.7
Sum	99.82	99.78	99.75
Ni	162	78	72
Rb	1.3	10.3	24.2
Ba	17	124	207
Sc	41	34	30
Th	0.2	1	2
U	<0.1	1.2	0.6
Nb	1.5	13.3	23.2
Ta	0.1	0.7	1.3
La	2.5	12.4	24.4
Ce	6	30.9	53.2
Pr	1.11	4.43	7.45
Sr	208.2	302.4	204.2
Nd	6.6	21	33.4
Zr	44.6	136.8	180.2
Hf	1.9	3.1	4.1
Sm	2.26	4.9	7.32
Eu	0.81	1.64	1.98
Gd	3.47	5.32	6.65
Tb	0.57	0.9	0.85
Dy	4.39	5.2	5.07
Y	24.2	31.2	24.6
Ho	0.87	1.07	0.9
Er	2.27	3.74	2.34
Tm	0.34	0.46	0.35
Yb	2.66	2.86	2.23
Lu	0.32	0.48	0.31
Co	45.8	48.4	47.7

The U-Pb analyses are available in the Supplementary data file labeled as U_Pb_data

Analytical data of zircons of TN-8 sample. In bold unused data to obtain igneous crystallization age. In italics data used for obtaining metamorphic age.

Grain Spot	U (ppm)	Th (ppm)	Th/U	$^{206}Pb^{*}$ (ppm)	$^{206}Pb^{c}$ %	Isotope ratios							Age (Ma)						%
						$^{207}Pb^{*}/^{235}U$	± (%)	$^{206}Pb^{*}/^{238}U$	± (%)	r	$^{207}Pb^{*}/^{206}Pb^{*}$	± (%)	$^{206}Pb/^{238}U$	±	$^{207}Pb/^{235}U$	±	$^{207}Pb/^{206}Pb$	±	Disc.
TN8A-1.1	311.84	298.96	0.99	73.88	-0.0086	3.664760	4.27	0.275558	4.19	0.98	0.096457	0.79	1573	58	1564	67	1557	15	-1
TN8A-2.1	187.77	131.55	0.72	45.30	-0.2316	3.708945	4.40	0.280520	4.24	0.96	0.095893	1.16	1598	60	1573	69	1546	22	-3
TN8A-3.1	141.40	95.90	0.70	34.36	-0.0072	3.760617	4.38	0.281979	4.19	0.96	0.096727	1.26	1605	59	1584	69	1562	24	-2
TN8A-4.1	**306.02**	**202.74**	**0.68**	**73.20**	**-0.4101**	**3.580865**	**4.28**	**0.277981**	**4.17**	**0.97**	**0.093429**	**0.95**	**1581**	**58**	**1545**	**66**	**1497**	**18**	**-5**
TN8A-5.1	*467.76*	*1.35*	*0.00*	*40.62*	*-0.0322*	*0.827344*	*4.38*	*0.100982*	*4.17*	*0.95*	*0.059421*	*1.33*	*620*	*25*	*612*	*27*	*583*	*29*	-6
TN8A-6.1	151.86	102.70	0.70	36.66	-0.2249	3.726523	4.41	0.280803	4.25	0.96	0.096251	1.20	1599	60	1577	70	1553	23	-3
TN8A-7.1	**76.46**	**44.10**	**0.60**	**17.78**	**0.2812**	**3.484211**	**4.84**	**0.269189**	**4.23**	**0.87**	**0.093878**	**2.34**	**1537**	**58**	**1524**	**74**	**1506**	**45**	**-2**
TN8A-8.1	144.31	96.45	0.69	34.70	-0.0124	3.749917	4.34	0.279594	4.19	0.96	0.097274	1.14	1593	59	1582	69	1572	21	-1
TN8A-9.1	196.10	194.53	1.02	47.67	-0.3124	3.754612	4.27	0.282864	4.18	0.98	0.096269	0.90	1610	59	1583	68	1553	17	-3
TN8A-10.1	272.65	199.83	0.76	65.45	-0.1560	3.721154	4.24	0.279313	4.17	0.98	0.096624	0.79	1592	59	1576	67	1560	15	-2
TN8A-11.1	**50.10**	**23.62**	**0.49**	**11.33**	**0.63**	**3.39221**	**4.99**	**0.26157**	**4.26**	**0.85**	**0.09406**	**2.56790**	**1498**	**57**	**1503**	**75**	**1509**	**49**	**1**
TN8A-12.1	**206.46**	**112.13**	**0.56**	**43.44**	**0.5436**	**3.121166**	**4.32**	**0.244524**	**4.18**	**0.97**	**0.092575**	**1.08**	**1410**	**53**	**1438**	**62**	**1479**	**21**	**5**
TN8D-1.1	**548.21**	**448.01**	**0.84**	**67.59**	**1.8169**	**1.603705**	**4.27**	**0.143272**	**4.17**	**0.98**	**0.081182**	**0.95**	**863**	**34**	**972**	**42**	**1226**	**19**	**42**
TN8D-2.1	**77.94**	**43.89**	**0.58**	**13.96**	**1.2807**	**2.503567**	**5.11**	**0.207471**	**4.23**	**0.83**	**0.087517**	**2.86**	**1215**	**47**	**1273**	**65**	**1372**	**55**	**13**
TN8D-3.1	**162.19**	**63.81**	**0.41**	**26.47**	**1.6614**	**2.274242**	**4.70**	**0.189178**	**4.26**	**0.91**	**0.087187**	**1.98**	**1117**	**44**	**1204**	**57**	**1365**	**38**	**22**
TN8D-4.1	**620.59**	**39.31**	**0.07**	**59.00**	**0.4587**	**0.998464**	**4.33**	**0.110626**	**4.17**	**0.96**	**0.065460**	**1.19**	**676**	**27**	**703**	**30**	**789**	**25**	**17**
TN8D-5.1	160.76	112.13	0.72	32.73	0.8827	3.005246	4.41	0.236278	4.21	0.95	0.092247	1.32	1370	52	1409	62	1472	25	8
TN8D-6.1	*506.01*	*1.86*	*0.00*	*44.23*	*-0.0626*	*0.842672*	*4.31*	*0.101740*	*4.17*	*0.97*	*0.060071*	*1.09*	*625*	*25*	*621*	*27*	*606*	*23*	-3
TN8D-7.1	*362.74*	*1.46*	*0.00*	*31.69*	*-0.0157*	*0.843290*	*4.47*	*0.101644*	*4.25*	*0.95*	*0.060172*	*1.40*	*624*	*25*	*621*	*28*	*610*	*30*	-2
TN8D-8.1	**186.45**	**84.73**	**0.47**	**31.48**	**1.29**	**2.33792**	**4.69**	**0.19594**	**4.32**	**0.92**	**0.08654**	**1.81647**	**1153**	**46**	**1224**	**57**	**1350**	**35**	**17**
TN8D-9.1	**621.94**	**558.55**	**0.93**	**52.36**	**1.34**	**0.87336**	**4.67**	**0.09728**	**4.17**	**0.89**	**0.06511**	**2.07101**	**598**	**24**	**637**	**30**	**778**	**44**	**30**
TN8D-10.1	**25.08**	**1.54**	**0.06**	**4.49**	**7.23**	**3.56472**	**22.45**	**0.20465**	**4.58**	**0.20**	**0.12625**	**21.94877**	**1200**	**50**	**1542**	**346**	**2048**	**388**	**71**
TN8D-11.1	**18.55**	**2.51**	**0.14**	**4.16**	**9.30**	**4.83960**	**9.31**	**0.25100**	**4.57**	**0.49**	**0.13960**	**8.02231**	**1444**	**59**	**1792**	**167**	**2225**	**140**	**54**
TN8F-1.1	**302.42**	**657.91**	**2.25**	**52.81**	**1.57**	**2.46146**	**4.58**	**0.20213**	**4.19**	**0.91**	**0.08832**	**1.83445**	**1187**	**45**	**1261**	**58**	**1389**	**36**	**17**
TN8F-2.1	177.56	98.25	0.57	35.46	1.0354	2.924457	4.53	0.231524	4.29	0.95	0.091610	1.45	1345	52	1388	63	1459	28	9
TN8F-3.1	529.73	380.28	0.74	97.55	0.7078	2.559554	4.39	0.214007	4.25	0.97	0.086743	1.10	1253	48	1289	57	1355	21	8
TN8F-4.1	*143.32*	*6.85*	*0.05*	*13.03*	*0.4030*	*0.888704*	*5.25*	*0.105366*	*4.22*	*0.80*	*0.061174*	*3.11*	*646*	*26*	*646*	*34*	*645*	*67*	0
TN8F-5.1	**209.02**	**63.51**	**0.31**	**31.70**	**1.98**	**1.89346**	**5.36**	**0.17394**	**4.22**	**0.79**	**0.07895**	**3.21751**	**1034**	**40**	**1079**	**58**	**1171**	**65**	**13**
TN8F-6.1	290.01	208.07	0.74	63.81	0.5098	3.232072	4.47	0.254697	4.18	0.94	0.092038	1.56	1466	55	1465	66	1468	30	0
TN8F-7.1	238.21	206.67	0.90	57.24	-0.1774	3.656743	4.34	0.279063	4.19	0.97	0.095039	1.13	1590	59	1562	68	1529	21	-4
TN8F-8.1	**488.38**	**298.59**	**0.63**	**65.69**	**1.78**	**1.72222**	**4.46**	**0.15566**	**4.18**	**0.94**	**0.08024**	**1.52855**	**933**	**36**	**1017**	**45**	**1203**	**31**	**29**
TN8F-9.1	223.23	105.34	0.49	42.76	1.4558	2.725791	4.60	0.221063	4.19	0.91	0.089426	1.85	1290	49	1336	61	1413	36	10
TN8F-10.1	*288.92*	*4.01*	*0.01*	*26.64*	*-0.0036*	*0.890757*	*4.63*	*0.107163*	*4.20*	*0.91*	*0.060286*	*1.95*	*656*	*26*	*647*	*30*	*614*	*42*	-6
TN8F-11.1	264.16	172.16	0.67	60.07	0.3426	3.402661	4.37	0.263522	4.18	0.96	0.093650	1.23	1511	56	1505	66	1501	24	0
TN8F-12.1	207.82	121.13	0.60	42.10	0.9777	2.949275	4.67	0.234595	4.25	0.91	0.091178	1.93	1361	52	1395	65	1450	37	7

Analytical data of zircons of P2A sample. In bold unused data to obtain age. In italics inherited zircon grains not used to obtain age.

Grain Spot	U (ppm)	Th (ppm)	Th/U	$^{206}Pb^{*}$ (ppm)	$^{206}Pb_{c}$ %	Isotope ratios							Age (Ma)						%
						$^{207}Pb^{*}/^{235}U$	± (%)	$^{206}Pb^{*}/^{238}U$	± (%)	r	$^{207}Pb^{*}/^{206}Pb^{*}$	± (%)	$^{206}Pb/^{238}U$	±	$^{207}Pb/^{235}U$	±	$^{207}Pb/^{206}Pb$	±	Disc.
P2A-1.1	**221.22**	**158.85**	**0.74**	**65.02**	**-0.22**	**5.34610**	**4.32**	**0.34170**	**4.22**	**0.98**	**0.11347**	**0.93035**	**1895**	**69**	**1876**	**81**	**1856**	**17**	**-2**
P2A-2.1	**106.48**	**76.75**	**0.74**	**23.26**	**-0.52**	**3.05851**	**4.55**	**0.25415**	**4.22**	**0.93**	**0.08728**	**1.69845**	**1460**	**55**	**1422**	**65**	**1367**	**33**	**-6**
P2A-3.1	173.47	136.72	0.81	30.36	0.41	2.23945	4.91	0.20289	4.48	0.91	0.08006	1.99145	1191	49	1193	59	1198	40	1
P2A-4.1	*104.04*	*77.02*	*0.76*	*34.14*	*-0.28*	*6.51932*	*4.48*	*0.38054*	*4.22*	*0.94*	*0.12426*	*1.47259*	*2079*	*75*	*2049*	*92*	*2018*	*26*	-3
P2A-5.1	266.74	139.11	0.54	44.24	0.10	2.02899	4.48	0.19255	4.20	0.94	0.07643	1.56851	1135	44	1125	50	1106	31	-3
P2A-6.1	881.15	190.44	0.22	141.54	-0.01	1.94484	4.26	0.18679	4.19	0.98	0.07552	0.76156	1104	42	1097	47	1082	15	-2
P2A-7.1	**502.78**	**6.91**	**0.01**	**94.20**	**-0.25**	**2.43981**	**4.29**	**0.21810**	**4.17**	**0.97**	**0.08113**	**1.01237**	**1272**	**48**	**1254**	**54**	**1225**	**20**	**-4**
P2A-8.1	503.11	161.98	0.33	82.07	-0.21	1.96305	4.28	0.18982	4.18	0.97	0.07501	0.95280	1120	43	1103	47	1069	19	-5
P2A-9.1	**895.33**	**196.42**	**0.23**	**79.17**	**2.37**	**1.03006**	**4.72**	**0.10204**	**4.17**	**0.88**	**0.07321**	**2.19816**	**626**	**25**	**719**	**34**	**1020**	**45**	**63**
P2A-10.1	**295.59**	**130.71**	**0.46**	**59.97**	**1.13**	**3.08244**	**4.33**	**0.23570**	**4.18**	**0.97**	**0.09485**	**1.12154**	**1364**	**51**	**1428**	**62**	**1525**	**21**	**12**
P2A-11.1	*90.02*	*85.19*	*0.98*	*25.22*	*-0.06*	*4.75423*	*4.61*	*0.32410*	*4.23*	*0.92*	*0.10640*	*1.80285*	*1810*	*67*	*1777*	*82*	*1738*	*33*	-4
P2A-12.1	*332.68*	*104.97*	*0.33*	*76.55*	*-0.01*	*3.44097*	*4.34*	*0.26724*	*4.18*	*0.96*	*0.09339*	*1.15986*	*1527*	*57*	*1514*	*66*	*1496*	*22*	-2

Analytical data of zircons of P2D sample. In bold unused data to obtain the age spectra.

Spot number	Ratios							Age (Ma)						%	f 206	Age (Ma)	±	Th	U	Pb	$^{232}Th/^{238}U$
	$^{207}Pb^*/^{235}U$	±	$^{206}Pb^*/^{238}U$	±	Rho 1	$^{207}Pb^*/^{206}Pb^*$	±	$^{206}Pb/^{238}U$	±	$^{207}Pb/^{235}U$	±	$^{207}Pb/^{206}Pb$	±	Disc.				ppm	ppm	ppm	
P-2D 1	2.31603	3.25	0.20552	3.06	0.94	0.08173	1.09	1205	37	1217	40	1239	14	3	0.0007	1229	36	216.5	515.4	181.8	0.42
P-2D 2	3.43865	4.85	0.26001	4.75	0.98	0.09592	1.02	1490	71	1513	73	1546	16	4	0.0004	1542	36	57.6	221.5	78.7	0.26
P-2D 3	2.76864	3.61	0.22588	2.85	0.79	0.08890	2.22	1313	37	1347	49	1402	31	6	0.0015	1542	36	22.2	77.3	24.5	0.29
P-2D 4	2.30292	3.39	0.20503	3.01	0.89	0.08146	1.56	1202	36	1213	41	1233	19	2	0.0014	1219	45	706.2	545.9	188.9	1.30
P-2D 5	2.55544	2.92	0.21891	2.19	0.75	0.08467	1.92	1276	28	1288	38	1308	25	2	0.0016	1286	42	127.2	129.5	47.7	0.99
P-2D 6	2.08715	4.02	0.19146	3.55	0.88	0.07906	1.88	1129	40	1145	46	1174	22	4	0.0023	1151	53	24.5	75.9	20.3	0.32
P-2D 7	2.11280	4.44	0.19261	4.03	0.91	0.07956	1.87	1135	46	1153	51	1186	22	4	0.0010	1164	56	34.6	118.4	31.0	0.29
P-2D 8	3.06795	2.62	0.24416	2.33	0.89	0.09113	1.21	1408	33	1425	37	1449	18	3	0.0004	1434	36	52.5	300.6	99.9	0.18
P-2D 9	2.92996	2.74	0.24031	2.36	0.86	0.08843	1.39	1388	33	1390	38	1392	19	0	0.0010	1390	40	220.5	252.0	90.2	0.88
P-2D 10	4.93173	8.04	0.30726	7.93	0.99	0.11641	1.29	1727	137	1808	145	1902	24	9	0.0016	1897	42	218.7	236.5	127.6	0.93
P-2D 11	3.47993	3.61	0.26191	3.42	0.95	0.09636	1.13	1500	51	1523	55	1555	18	4	0.0010	1545	38	29.2	149.8	52.6	0.20
P-2D 12	2.25394	4.86	0.20007	4.59	0.94	0.08171	1.60	1176	54	1198	58	1238	20	5	0.0012	1221	53	62.3	111.7	34.9	0.56
P-2D 13	3.22505	13.95	0.26193	3.10	0.22	0.08930	13.6	1500	47	1463	204	1411	192	-6	0.0004	1497	82	44.4	349.6	118.7	0.13
P-2D 14	2.65987	5.48	0.22405	5.31	0.97	0.08610	1.33	1303	69	1317	72	1340	18	3	0.0009	1335	47	130.2	479.7	142.9	0.27
P-2D 15	2.25035	3.49	0.20340	2.91	0.83	0.08024	1.92	1194	35	1197	42	1203	23	1	0.0015	1197	49	33.2	96.0	26.7	0.35
P-2D 16	1.83042	3.04	0.17566	2.29	0.75	0.07557	1.99	1043	24	1056	32	1084	22	4	0.0025	1052	39	156.0	382.1	92.8	0.41
P-2D 17	2.50104	4.35	0.21877	3.78	0.87	0.08292	2.17	1275	48	1272	55	1267	27	-1	0.0060	1271	61	53.1	87.3	27.9	0.61
P-2D 18	3.48319	2.28	0.26517	1.90	0.83	0.09527	1.27	1516	29	1523	35	1533	19	1	0.0007	1525	35	67.8	170.8	63.0	0.40
P-2D 19	1.93246	5.23	0.18328	4.89	0.93	0.07647	1.87	1085	53	1092	57	1107	21	2	0.0024	1099	59	47.2	96.0	26.7	0.50
P-2D 20	2.33403	4.80	0.20906	4.26	0.89	0.08097	2.21	1224	52	1223	59	1221	27	0	0.0026	1222	64	36.6	69.1	20.6	0.53
P-2D 21	2.70704	6.37	0.22734	5.64	0.89	0.08636	2.95	1321	75	1330	85	1346	40	2	0.0032	1336	87	35.9	36.1	16.2	1.00
P-2D 22	5.93130	3.06	0.34740	2.75	0.90	0.12383	1.35	1922	53	1966	60	2012	27	4	0.0002	1993	42	85.6	269.1	163.1	0.32
P-2D 23	2.39589	2.43	0.21139	2.03	0.84	0.08220	1.34	1236	25	1241	30	1250	17	1	0.0007	1242	35	52.5	139.6	49.1	0.38
P-2D 24	3.60256	3.99	0.27019	3.82	0.96	0.09670	1.16	1542	59	1550	62	1561	18	1	0.0005	1559	40	51.1	158.2	71.6	0.33
P-2D 25	5.82112	3.11	0.34723	2.91	0.94	0.12159	1.09	1921	56	1950	61	1980	22	3	0.0010	1972	36	74.6	124.3	80.6	0.60
P-2D 26	4.89706	5.00	0.33021	4.78	0.96	0.10756	1.45	1839	88	1802	90	758	26	-5	0.0007	1768	52	29.1	72.6	39.9	0.40
P-2D 27	2.71883	3.21	0.22982	2.86	0.89	0.08580	1.45	1334	38	1334	43	1334	19	0	0.0020	1334	44	63.5	59.8	26.6	1.07
P-2D 28	2.92064	2.75	0.24103	2.31	0.84	0.08788	1.50	1392	32	1387	38	1380	21	-1	0.0012	1386	41	31.5	90.3	35.0	0.35
P-2D 29	5.02582	3.44	0.32843	3.09	0.90	0.11098	1.51	1831	57	1824	63	1816	27	-1	0.0018	1819	48	24.4	34.9	20.3	0.70
P-2D 30	3.35308	3.63	0.26043	3.36	0.92	0.09338	1.39	1492	50	1494	54	1496	21	0	0.0015	1495	45	28.4	72.0	33.5	0.40
P-2D 31	3.44272	3.12	0.26249	2.68	0.86	0.09512	1.60	1503	40	1514	47	1530	24	2	0.0011	1519	46	38.2	96.9	38.2	0.40
P-2D 32	3.68852	2.94	0.27554	2.67	0.91	0.09709	1.24	1569	42	1569	46	1569	19	0	0.0004	1569	40	74.2	223.1	91.8	0.33
P-2D 33	2.36693	2.86	0.21052	2.42	0.85	0.08154	1.53	1232	30	1233	35	1235	19	0	0.0009	1233	40	68.2	138.1	44.2	0.50
P-2D 34	**5.17233**	**9.43**	**0.33668**	**7.77**	**0.82**	**0.11142**	**5.34**	**1871**	**145**	**1848**	**174**	**1823**	**97**	**-3**	**0.0017**	**1841**	**150**	**23.9**	**15.0**	**9.6**	**1.60**
P-2D 35	2.71920	3.12	0.23030	2.84	0.91	0.08563	1.30	1336	38	1334	42	1330	17	0	0.0009	1332	41	18.5	125.4	38.9	0.15
P-2D 36	2.66804	5.99	0.22778	5.38	0.90	0.08495	2.64	1323	71	1320	79	1314	35	-1	0.0021	1318	80	36.6	33.6	13.9	1.10
P-2D 37	6.57853	2.34	0.37650	2.11	0.90	0.12673	1.01	2060	43	2056	48	2053	21	0	0.0003	2054	32	190.9	230.5	145.5	0.83
P-2D 38	3.06030	4.58	0.25014	4.45	0.97	0.08873	1.12	1439	64	1423	65	1398	16	-3	0.0004	1404	41	163.0	318.9	120.4	0.51
P-2D 39	2.90497	3.65	0.23974	3.26	0.89	0.08788	1.63	1385	45	1383	50	1380	22	0	0.0012	1382	50	29.9	79.4	27.4	0.38
P-2D 40	4.65571	3.66	0.31241	3.37	0.92	0.10808	1.44	1753	59	1759	64	1767	25	1	0.0008	1764	47	50.1	92.8	46.0	0.54
P-2D 41	5.31420	2.96	0.33565	2.60	0.88	0.11483	1.42	1866	49	1871	55	1877	27	1	0.0005	1874	44	97.8	99.0	64.5	1.00
P-2D 42	4.74930	5.78	0.31140	4.67	0.81	0.11061	3.42	1748	82	1776	103	1810	62	3	0.0029	1783	94	31.6	38.2	22.2	0.83
P-2D 43	4.89538	5.78	0.32067	4.74	0.82	0.11072	3.31	1793	85	1801	104	1811	60	1	0.0025	1804	94	44.8	31.9	21.0	1.41
P-2D 44	2.54094	5.83	0.22224	5.03	0.86	0.08292	2.96	1294	65	1284	75	1267	37	-2	0.0031	1280	82	12.1	58.8	14.5	0.21
P-2D 45	2.14995	2.66	0.19942	2.13	0.80	0.07819	1.59	1172	25	1165	31	1152	18	-2	0.0004	1165	37	139.5	310.2	103.2	0.45

Continue...

Continuation

Spot number	Ratios							Age (Ma)						%	f 206	Age (Ma)	±	Th	U	Pb	$^{232}Th/^{238}U$
	$^{207}Pb^*/^{235}U$	±	$^{206}Pb^*/^{238}U$	±	Rho 1	$^{207}Pb^*/^{206}Pb^*$	±	$^{206}Pb/^{238}U$	±	$^{207}Pb/^{235}U$	±	$^{207}Pb/^{206}Pb$	±	Disc.				ppm	ppm	ppm	
P-2D 46	2.30179	2.80	0.20507	2.28	0.81	0.08141	1.63	1203	27	1213	34	1231	20	2	0.0006	1213	40	43.8	141.3	46.9	0.31
P-2D 47	5.45998	3.30	0.34329	2.88	0.87	0.11535	1.61	1902	55	1894	63	1885	30	-1	0.0013	1890	50	54.3	68.6	43.4	0.80
P-2D 48	2.15679	4.24	0.19839	3.39	0.80	0.07885	2.55	1167	40	1167	50	1168	30	0	0.0018	1167	59	63.9	77.4	28.5	0.83
P-2D 49	1.95465	5.41	0.18475	4.87	0.90	0.07673	2.33	1093	53	1100	59	1114	26	2	0.0020	1104	68	75.5	59.8	22.2	1.27
P-2D 50	1.68812	3.68	0.16981	3.28	0.89	0.07210	1.69	1011	33	1004	37	989	17	-2	0.0010	1001	46	82.6	244.5	65.6	0.34
P-2D 51	4.45100	5.64	0.30822	5.48	0.97	0.10474	1.33	1732	95	1722	97	1710	23	-1	0.0011	1712	48	66.2	104.3	64.8	0.64
P-2D 52	2.37013	5.83	0.21107	5.43	0.93	0.08144	2.13	1235	67	1234	72	1232	26	0	0.0014	1233	69	26.5	68.7	26.9	0.39
P-2D 53	6.56498	3.43	0.37498	2.91	0.85	0.12698	1.82	2053	60	2055	70	2057	37	0	0.0007	2055	55	60.4	48.9	42.6	1.24
P-2D 54	5.93850	4.12	0.35527	3.91	0.95	0.12123	1.31	1960	77	1967	81	1974	26	1	0.0004	1973	44	55.3	189.4	116.9	0.29
P-2D 55	2.16693	3.95	0.20065	3.69	0.93	0.07833	1.43	1179	43	1170	46	1155	17	-2	0.0003	1163	46	22.3	267.3	89.5	0.08
P-2D 56	4.64295	3.75	0.31261	3.29	0.88	0.10772	1.79	1754	58	1757	66	1761	31	0	0.0008	1759	55	15.4	47.9	28.2	0.32
P-2D 57	3.58230	3.25	0.27256	3.00	0.92	0.09532	1.26	1554	47	1546	50	1534	19	-1	0.0004	1539	41	33.4	118.3	57.8	0.28
P-2D 58	5.84630	4.20	0.35228	3.77	0.90	0.12036	1.85	1945	73	1953	82	1962	36	1	0.0012	1958	59	96.9	115.4	80.0	0.85
P-2D 59	2.14794	5.41	0.20342	4.83	0.89	0.07658	2.45	1194	58	1164	63	1110	27	-8	0.0020	1149	71	27.7	53.6	18.9	0.52
P-2D 60	3.57354	4.37	0.27076	4.06	0.93	0.09572	1.61	1545	63	1544	67	1542	25	0	0.0007	1543	53	30.5	114.0	58.8	0.27
P-2D 61	4.82954	2.59	0.32030	2.30	0.89	0.10936	1.20	1791	41	1790	46	1789	21	0	0.0007	1789	37	178.0	83.0	70.3	2.16
P-2D 62	**4.93288**	**6.31**	**0.31771**	**4.87**	**0.77**	**0.11261**	**4.02**	**1779**	**87**	**1808**	**114**	**1842**	**74**	**3**	**0.0013**	**1811**	**110**	**6.1**	**9.5**	**5.7**	**0.64**
P-2D 63	4.67546	4.03	0.31262	3.56	0.88	0.10847	1.87	1754	62	1763	71	1774	33	1	0.0012	1768	58	82.1	56.3	41.0	1.47
P-2D 64	2.62481	4.75	0.22364	4.42	0.93	0.08512	1.75	1301	57	1308	62	1318	23	1	0.0022	1313	57	102.3	73.9	33.9	1.39
P-2D 65	1.93294	5.29	0.18483	4.58	0.86	0.07585	2.66	1093	50	1093	58	1091	29	0	0.0022	1092	70	31.0	55.3	19.2	0.56
P-2D 66	2.13990	5.82	0.19724	4.81	0.83	0.07869	3.27	1160	56	1162	68	1164	38	0	0.0031	1162	80	14.2	44.4	15.5	0.32
P-2D 67	2.34276	3.93	0.20840	3.36	0.86	0.08153	2.03	1220	41	1225	48	1234	25	1	0.0013	1227	55	36.8	73.8	28.8	0.50
P-2D 68	3.58297	1.87	0.27016	1.55	0.83	0.09619	1.05	1542	24	1546	29	1551	16	1	0.0004	1547	29	72.0	262.1	125.1	0.28
P-2D 69	6.19497	5.70	0.36503	4.93	0.86	0.12309	2.86	2006	99	2004	114	2001	57	0	0.0014	2003	87	17.3	11.6	9.8	1.51
P-2D 70	2.36512	5.90	0.21095	5.34	0.90	0.08132	2.52	1234	66	1232	73	1229	31	0	0.0008	1231	76	18.1	43.7	17.8	0.42
P-2D 71	2.69138	4.69	0.23106	4.37	0.93	0.08448	1.71	1340	59	1326	62	1304	22	-3	0.0007	1314	57	51.4	132.1	50.9	0.39
P-2D 72	2.13668	10.33	0.19568	10.14	0.98	0.07919	1.97	1152	117	1161	120	1177	23	2	0.0038	1174	72	122.1	233.3	61.6	0.53
P-2D 73	2.35119	5.55	0.20865	4.42	0.80	0.08173	3.36	1222	54	1228	68	1239	42	1	0.0020	1228	79	19.5	27.3	9.6	0.72
P-2D 74	3.71360	3.99	0.28159	3.78	0.95	0.09565	1.28	1599	60	1574	63	1541	20	-4	0.0004	1551	45	55.7	255.0	100.8	0.22
P-2D 75	4.84178	3.29	0.31871	2.71	0.83	0.11018	1.86	1783	48	1792	59	1802	33	1	0.0012	1795	53	38.4	45.7	25.1	0.85
P-2D 76	3.43238	2.62	0.26435	2.15	0.82	0.09417	1.50	1512	32	1512	40	1512	23	0	0.0009	1512	41	72.1	123.3	53.0	0.59
P-2D 77	5.58509	3.17	0.33729	3.03	0.96	0.12009	0.92	1874	57	1914	61	1958	18	4	0.0004	1950	31	243.5	179.6	114.9	1.37
P-2D 78	5.40112	4.55	0.35032	3.84	0.84	0.11182	2.44	1936	74	1885	86	1829	45	-6	0.0023	1864	73	25.7	35.8	17.3	0.72
P-2D 79	3.72752	2.82	0.27784	2.37	0.84	0.09730	1.52	1580	37	1577	44	1573	24	0	0.0013	1576	43	33.1	76.5	32.6	0.44
P-2D 80	4.61513	2.80	0.31280	2.27	0.81	0.10701	1.64	1754	40	1752	49	1749	29	0	0.0015	1751	46	89.0	70.0	40.4	1.28
P-2D 81	2.35619	5.17	0.21206	4.87	0.94	0.08058	1.73	1240	60	1229	64	1211	21	-2	0.0007	1219	58	201.6	320.2	107.2	0.63
P-2D 82	2.96770	5.74	0.23279	5.36	0.93	0.09246	2.06	1349	72	1399	80	1477	30	9	0.0025	1445	65	10.8	56.3	22.4	0.19
P-2D 83	3.22163	8.61	0.25483	8.51	0.99	0.09169	1.31	1463	125	1462	126	1461	19	0	0.0030	1461	49	129.8	299.1	94.1	0.44
P-2D 84	3.06025	2.57	0.24445	2.15	0.84	0.09079	1.41	1410	30	1423	37	1442	20	2	0.0018	1426	38	89.7	268.7	96.6	0.34
P-2D 85	1.97675	2.91	0.18671	2.38	0.82	0.07678	1.68	1104	26	1108	32	1116	19	1	0.0010	1108	39	21.2	140.0	40.1	0.15
P-2D 86	1.64161	6.69	0.16398	6.39	0.95	0.07261	2.00	979	63	986	66	1003	20	2	0.0016	995	66	144.8	255.1	63.9	0.57
P-2D 87	2.81051	7.46	0.23047	7.16	0.96	0.08845	2.12	1337	96	1358	101	1392	29	4	0.0012	1383	72	37.5	73.1	28.9	0.52
P-2D 88	5.81363	5.04	0.36215	4.46	0.88	0.11643	2.36	1992	89	1948	98	1902	45	-5	0.0030	1924	75	178.3	211.0	106.9	0.85
P-2D 89	5.22634	3.14	0.32724	2.83	0.90	0.11583	1.37	1825	52	1857	58	1893	26	4	0.0007	1878	43	62.3	96.9	58.5	0.65
P-2D 90	**1.94655**	**15.75**	**0.18310**	**14.4**	**0.91**	**0.07710**	**6.47**	**1084**	**156**	**1097**	**173**	**1124**	**73**	**4**	**0.0024**	**1106**	**190**	**7.1**	**24.7**	**7.9**	**0.29**